

MoRoCo: An Online Topology-Adaptive Framework for Multi-Operator Multi-Robot Coordination under Restricted Communication

Zhuoli Tian, Yanze Bao, Yuyang Zhang, and Meng Guo*

Abstract—Fleets of autonomous robots are increasingly deployed with multiple human operators in communication-restricted environments for exploration and intervention tasks such as subterranean inspection, reconnaissance, and search-and-rescue. In these settings, communication is often limited to short-range ad-hoc links, making it difficult to coordinate exploration while supporting online human-fleet interactions. Existing work on multi-robot exploration largely focuses on information gathering itself, but pays limited attention to the fact that operators and robots issue time-critical requests during execution. These requests may require different communication structures, ranging from intermittent status delivery to sustained video streaming and teleoperation. To address this challenge, this paper presents MoRoCo, an online topology-adaptive framework for multi-operator multi-robot coordination under restricted communication. MoRoCo is built on a latency-bounded intermittent communication backbone that guarantees a prescribed delay for information collected by any robot to reach an operator, together with a detach-and-rejoin mechanism that enables online team resizing and topology reconfiguration. On top of this backbone, the framework instantiates request-consistent communication subgraphs to realize different modes of operator-robot interaction by jointly assigning robot roles, positions, and communication topology. It further supports the online decomposition and composition of these subgraphs using only local communication, allowing multiple requests to be serviced during exploration. The framework extends to heterogeneous fleets, multiple teams, and robot failures. Extensive human-in-the-loop simulations and hardware experiments demonstrate effective and reliable coordination under restricted communication.

Index Terms—Multi-robot systems, human-robot interaction, exploration, coordination, ad-hoc networks, communication constraint

I. INTRODUCTION

Autonomous robots such as unmanned aerial vehicles (UAVs) and ground vehicles (UGVs) are becoming common companions of human operators in various scenarios, especially to explore unknown and hazardous sites before entry, or search and rescue after earthquakes, see [1], [2]. The robots become extended eyes and arms of the operators by fusing their perception results to the operators and performing actions as instructed by the operators. Existing strategies for collaborative exploration in [3]–[6] often assume all-to-all communication among the robots. In other words, any local observation by one robot is immediately available to others, which is equivalent to one robot with multiple moving sensors. This is however impractical in aforementioned scenes where the communication facilities are unavailable or severely degraded. In such cases, the robot-robot and robot-operator

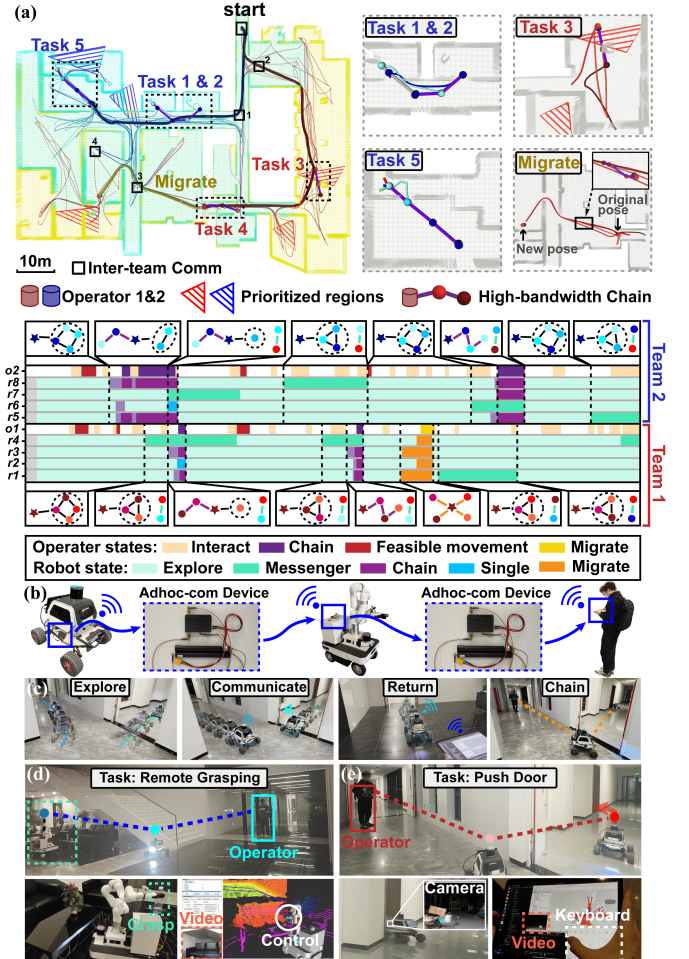


Fig. 1. Illustration of the considered scenario, where multiple operators and robots are deployed in an unknown and communication-restricted environment for exploration and task execution. (a) Simulation of 2 operators and 8 robots collaboratively exploring a large-scale environment, while accomplishing 5 tasks via splitting and merging embedded communication graphs; (b) Hardware experiments of 2 operators and 4 robots, with ad-hoc network devices for local communication in close proximity; (c) Intermittent communication protocol that ensures bounded-latency information flow between operators and robots; (d)–(e) Online request fulfillment via changing the communication topology for video streaming and teleoperation.

communication is often limited to ad-hoc networks in close proximity. This imposes great challenges for the operators to coordinate, supervise and interact with the fleet, as communications would not be feasible unless actively planned.

Furthermore, the role of the human operator and the online interaction with the fleet during exploration are less studied and mostly replaced by a static base station for visualization.

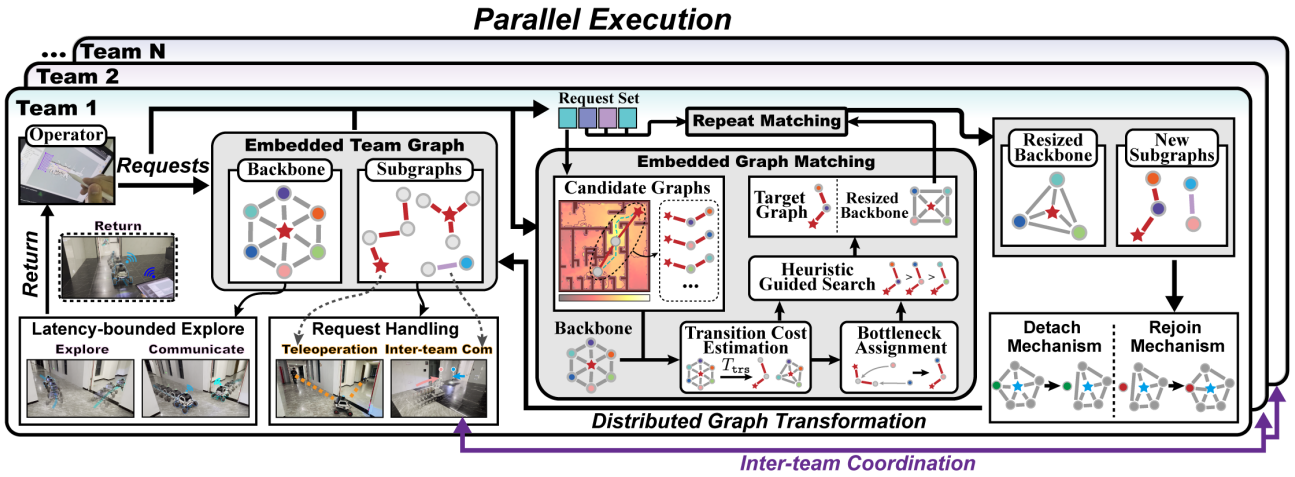


Fig. 2. Overall framework of MOROCO for multi-team human–robot coordination under restricted communication. Multiple teams of operator and robots simultaneously explore the environment and fulfill several online requests, following the embedded communication graphs under the intermittent communication protocol (Left); The embedded graph is optimized and matched against different targeted graphs given the current graph and the set of active requests (Middle); The resulting subgraphs are realized by the proposed detach-and-rejoin mechanism via only local coordination (Right).

However, under restricted communication, the operator might be *completely unaware* of the progress and results of the ongoing exploration if none of the robots actively return to the operator to relay such information. Consequently, the operator can not supervise the exploration task in real-time, e.g., checking the system status such as battery and liveness; and dynamically adjusting the priorities of the areas to be explored. In addition, as shown in Fig. 1, the operator often needs direct access to the video stream and control of a particular robot, e.g., to inspect certain regions close-up for important semantic features that are otherwise overlooked during exploration; or assist a robot through tough terrain via manual control. In another direction, the robots often need confirmation from the operator regarding actions or detected features, or immediate assistance. For these interactions, a *reliable and consistent information flow* is often required from the operator to the robot even during motion, which is particularly challenging in unknown environments without global communication.

To address these challenges, this work introduces **MoRoCo**, an online topology-adaptive framework for coordination, supervision, and interaction in multi-operator multi-robot systems operating in unknown environments under restricted communication. Seven types of bilateral and multi-modal interactions that arise during exploration are explicitly modeled. As outlined in Fig. 2, MoRoCo is built on a latency-bounded intermittent communication backbone that mediates all request delivery using only local communication. This backbone ensures that information gathered by any robot reaches an operator within a prescribed latency bound by coordinating successive communication events in time, location, and message content. A detach-and-rejoin procedure enables dynamic resizing of the fleet while preserving this communication objective. Each request type is further associated with a desired communication structure, such as a jointed wheel, line, or star. Building on the backbone, MoRoCo instantiates request-consistent embedded graphs that specify robot roles, positions, and communication topology for different interaction modes. To realize these graphs online, the framework employs a graph-matching-based request-

instantiation procedure that maps the current embedded graph to an executable target graph. In the presence of multiple simultaneous requests, an online feasible coordination policy incrementally decomposes the fleet into subgraphs that service individual requests, and later recomposes these subgraphs into larger exploration graphs upon completion. In this way, MoRoCo unifies collaborative exploration, online request handling, and communication-topology adaptation under intermittent connectivity. Moreover, the framework generalizes to heterogeneous fleets, and is demonstrated to handle exploration uncertainty and robot failures. Extensive human-in-the-loop simulations are conducted with more than 10 robots and 3 operators in typical office environments and subterranean caves of varying scales. In addition, hardware experiments are performed with a fleet of 4 ground vehicles and 2 operators in indoor environments.

The main contributions are threefold: (I) a structured formulation for multi-operator multi-robot systems operating in unknown environments under restricted communication, which captures seven explicit bilateral and multi-modal request types arising between robots and operators during exploration; (II) the proposed MoRoCo framework, which combines latency-bounded intermittent communication, collaborative exploration, and online request fulfillment through topology-adaptive coordination; and (III) a graph-based realization mechanism based on embedded-graph instantiation, matching, decomposition, and composition, together with framework-level guarantees on executable online request servicing and restoration of the exploration backbone.

II. RELATED WORK

A. Collaborative Exploration

The problem of collaborative exploration has a long history in robotics, as partially summarized in Table I. The frontier-based method from [7] introduces an intuitive yet powerful metric for guiding the exploration. Originally for a single robot, it was extended to multi-robot teams by assigning frontiers for concurrent exploration: e.g., greedily to the nearest robot by distance [8], centralized assignment via Voronoi

partitioning [9], distributed and sequential auction [3], multi-vehicle routing for optimal sequences [5], or based on expected information gain [6], [10], [11]. More recent learning-based methods [12], [13] leverage learned heuristics to prioritize frontiers or predict the unexplored map directly. Inter-robot communication is crucial for collaboration, enabling coordinated planning and avoiding redundant exploration. With known relative coordinates, map merge can be efficiently and accurately done [14]; otherwise, advanced methods like feature matching or geometric optimization are needed [15]. Work like ROAM [16] proposes a decentralized optimization scheme for consistency, and SlideSLAM [17] enables map fusion via semantic labelling and matching. However, these works all assume that robots can exchange information via wireless communication *perfectly and instantly* at all time. Thus, all robots always have access to the same global map and the same set of frontiers. This is impractical or infeasible without pre-installed communication infrastructures. As discussed in [18], due to obstructions in subterranean environments [19], [20] or indoor structures [21], inter-robot communication is severely limited both in range and reliability. Consequently, these approaches are not suitable for communication-constrained and unknown scenarios.

B. Limited Communication

To overcome the challenge of limited communication, many recent works focus on the joint planning of inter-robot communication and autonomous exploration. A straightforward solution is to establish a communication network covering the entire environment by pre-deploying communication devices [9], [22]. However, this approach is limited to known or small-scale environments and cannot be applied to large-scale unknown scenarios. A more practical approach designs exploration strategies that explicitly account for communication constraints [23]. Systematic techniques for mobility-communication networks have been developed, such as formulating a mixed integer program for the DARPA subterranean challenge [2]. Other methods include a Riemannian optimization approach for efficient exploration [16], a reinforcement learning strategy with one-hop communication [24], [25], and distributed optimization for semantic mapping and its representation to limit communication overhead [16].

Moreover, as partially summarized in Table I, different intermittent communication strategies address various performance metrics, such as the “Zonal and Sneakernet” relay algorithm [26]; the four-state strategy including explore, meet, sacrifice, relay [27]; distributed relay task assignment [28]; centralized optimization of rendezvous points [29]; and predicting robot positions via communication unavailability [30]. Fully distributed protocols for intermittent communication between robot pairs have also been proposed [31]. Conversely, some work imposes fully-connected communication networks at all times via collaborative motion planning [32] or by placing front and relay nodes to ensure a lower-bounded bandwidth [33], [34]. Droppable radios are used as communication relays between robots and a static base station [35], [36]. Recent work also proposes efficient map representations to

TABLE I
COMPARISON WITH RELATED WORK.

Method	Pre-inst. infra.	Interm. comm.	Human int.	Bound Lat.	Diff. Top.	Multi teams
Racer [5]	×	×	×	×	×	×
CURE [9]	✓	×	×	×	×	×
Achord [35]	✓ [†]	✓	×	×	✓	×
Madcat [36]	✓ [†]	✓	✓	×	✓	×
RELINK [34]	×	×	×	✓	✓	×
iHERO [38]	×	✓	✓	✓	×	×
JSSP [39]	×	✓	×	×	×	×
Corah [40]	×	✓	×	×	×	×
Realm [41]	×	×	×	✓	✓	×
MoRoCo (Ours)	×	✓	✓	✓	✓	✓

[†]Uses droppable beacons during online execution.

reduce communication overhead [37], while others tackle the hard constraint of lower-bounded information latency for all robots [38]. It is important to note that the aforementioned methods typically assume a static base station and consider *only one communication mode*, either intermittent communication or full connectivity. Thus, these approaches are limited when different modes are required for varying bandwidth, latency and topology. More importantly, they mostly neglect the crucial role of human operators and the potential online interactions between the operators and the fleet.

C. Human-Fleet Interaction

Indeed, the human operator plays *an indispensable role* in the operation of robotic fleets, even when these systems exhibit significant autonomous capabilities [42]. In practice, operators must not only monitor the fleet status online but also intervene when critical decisions or risky actions arise, while robots may require confirmation or direct assistance in unforeseen situations. Most existing work overlooks such bilateral interaction and instead assumes a static base station for visualization [2], [20], [29], [30], [35], resulting in rather uniform fleet behaviors until exploration is completed. An interactive exploration strategy was proposed in [38], but it is limited to simple exploration tasks and a single communication mode. Recent studies investigate richer interaction paradigms, including multi-modal inputs such as voice, gesture, gaze, and touch [36], as well as AR-based interfaces for immersive real-time supervision and drag-and-drop commands [43]. Joysticks and wristbands have also been used to support multi-robot supervision while monitoring operator workload [44]. However, these approaches typically rely on *consistent and reliable* communication between the operators and the fleet. These bilateral and online interactions bring numerous challenges for communication-constrained scenarios, which are not yet addressed formally in the literature: e.g., how to ensure a timely exchange between the operators and the fleet including newly explored map and requests; how to choose different modes of communication such as intermittent or rigid, to fulfill different requests and switch between modes.

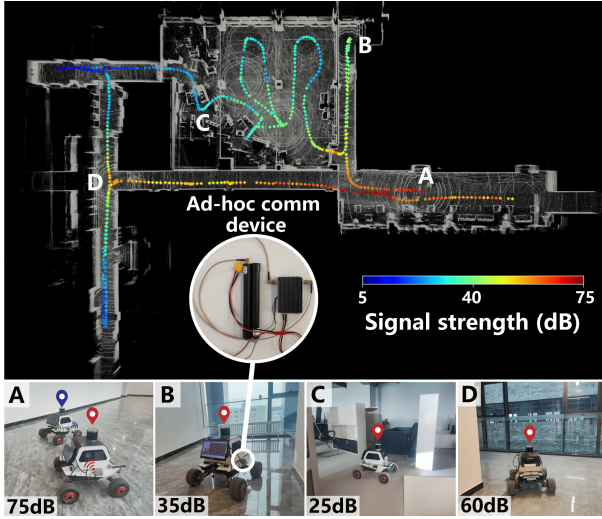


Fig. 3. The measured signal strength in an office environment via the ad-hoc communication network (Top) at different robot positions (Bottom).

III. PROBLEM DESCRIPTION

A. Multi-operator-robot Teams

Consider a 3D workspace $\mathcal{A} \subset \mathbb{R}^3$, of which its map including the boundary, freespace and obstacles are all unknown. To obtain a complete map and features within the workspace, in total $K > 0$ operator-robot teams $\mathcal{T} \triangleq \{\mathcal{T}_1, \dots, \mathcal{T}_K\}$ are deployed into the workspace. Each team \mathcal{T}_k consists of one human operator h_k and a small fleet of autonomous robots \mathcal{N}_k such as UAVs and UGVs, i.e., $\mathcal{T}_k \triangleq \{h_k\} \cup \mathcal{N}_k$. In other words, there are K operators and N robots in total, i.e., $N \triangleq \sum_{k \in \mathcal{K}} N_k$ with $\mathcal{N} \triangleq \bigcup_{k \in \mathcal{K}} \mathcal{N}_k$ and $\mathcal{K} \triangleq \{1, \dots, K\}$. As shown in Fig. 1 and 3, each robot $i \in \mathcal{N}$ is equipped with various sensors such as IMU, Lidar and RGBD cameras; and actuators to move around the workspace, which allows for simultaneous localization and mapping (SLAM) as follows.

Definition 1. Each robot is capable of simultaneous localization and mapping (SLAM) with collision avoidance, i.e.,

$$(M_i^+, p_i^+, \tau_i) \triangleq \text{SLAM}(p_i, p_g, M_i, \mathcal{A}), \quad (1)$$

where $\text{SLAM}(\cdot)$ is a generic SLAM module; $M_i(t) \subset \mathcal{A}$ is the local map of robot $i \in \mathcal{N}$ at time $t \geq 0$; $p_i(t) \in M_i$ is the pose of robot i ; $p_g \in M_i$ is a goal pose within M_i ; $\tau_i \subset M_i$ is the collision-free path from $p_i(t)$ to p_g ; $M_i^+ \subset \mathcal{A}$ is the updated map after traversing the path at time $t' > t$; and $p_i^+(t')$ is its updated pose, close to p_g if the navigation is successful. ■

On the other hand, the operators $h_k \in \mathcal{T}_k$ can *not* build a map, but can localize themselves with pose $p_h^k \in \mathcal{A}$ and move within their local maps M_h^k , i.e., $p_h^k(t) \in M_h^k(t) \subset \mathcal{A}$ for all $t \geq 0$ and $k \in \mathcal{K}$. Thus, it is essential that the operators to communicate with the robots to obtain their local maps.

Remark 1. The exact representation of the map depends on the underlying algorithm and software used for SLAM, e.g., the occupancy map in [45], or the semantic map in [46]. More details can be found in the numerical experiments. ■

B. Limited Inter-operator-robot Communication

Furthermore, as shown in Fig. 3, each robot and operator is equipped with a wireless communication unit for robot-

robot-operator information exchange, e.g., ad-hoc networks, UWB, radio or 5G network [2], [34]. The following model of communication is applied to the robotic fleet and operators.

Definition 2. Robot $i \in \mathcal{N}$ can communicate with robot $j \in \mathcal{N}$ at time $t > 0$, if the communication quality such as SNR is above a certain threshold, i.e.,

$$(D_i^+, D_j^+) \triangleq \text{Com}(D_i, D_j), \quad \text{if } \text{Qual}(p_i, p_j, \mathcal{A}) > \delta; \quad (2)$$

where $\text{Com}(\cdot)$ is the communication module; $D_i(t) \in \mathcal{D}$ is the local data at robot i at $t \geq 0$, similar for robot j ; \mathcal{D} includes map data, video stream, coordination messages and requests; $\text{Qual}(\cdot)$ evaluates the quality given positions and workspace; $\delta > 0$ is a lower bound on the quality; and $D_i^+(t)$, $D_j^+(t)$ are the updated data after communication. ■

By default, $(p_i, M_i) \in D_i$ holds for all robots and operators. Denote by $\mathcal{C}_i(t) \subset \mathcal{N}$ the set of robots that robot i can communicate with at time t under Def. 2. The operator-robot and operator-operator communications are defined similarly and omitted for brevity. Moreover, several communicating robots or operators can form a communication chain to relay information reliably and consistently.

Definition 3. A *communication chain* from robot $i_0 \in \mathcal{N}$ to the operator h at time $t \geq 0$ is given by:

$$\overline{i_h} \triangleq i_0 i_1 \dots i_\ell \dots i_L h, \quad (3)$$

where neighboring nodes $i_\ell \in \mathcal{C}_{i_{\ell+1}}(t)$ satisfy the condition in (2), $\forall \ell \in \{0, \dots, L-1\}$; and $i_L \in \mathcal{C}_h(t)$. ■

Remark 2. The above two communication modes are useful for different purposes: the pairwise communication by (2) is suitable for intermittent data exchange, while the communication chain by (3) is essential for an operator to have a consistent and reliable access to a robot for a duration. ■

C. Operator-fleet Online Interaction

Both the operators and the robots are capable of sending and receiving online *requests* to each other via the communication module above. More specifically, as summarized in Table II, seven types of requests are considered across three cases.

Operator-robot requests. The operators can send four types of requests $\xi_{1,2,3,4}^k$. (I) Intra-team latency constraint $\{\xi_1^k\}$. The operator h_k must obtain the local maps of all robots in its team \mathcal{T}_k with a latency smaller than a given threshold $T_h^k > 0$ at all times, i.e., $\bigcup_{i \in \mathcal{N}_k} M_i(t) \subset M_h^k(t + T_h^k)$, $\forall t \geq 0$. This means the explored map by any robot must be known to the operator h_k latest by time $t + T_h^k$. This request remains active once issued; (II) Prioritized or avoided region $\{\xi_2^k\}$. A certain region $\xi_2^k \subset \mathcal{A}$ should be prioritized or avoided during exploration by team \mathcal{N}_k . Fulfilled once the locations are all explored; (III) Operator movement $\{\xi_3^k\}$. The operator h_k requests to move to a desired location $p_h^{k,*}$. Fulfilled when the operator reaches $p_h^{k,*}$; (IV) Remote access or tele-operation $\{\xi_4^k\}$. The operator h_k requests remote access to robot $i^* \in \mathcal{N}_k$ at location p^* for duration $T_{i^*} > 0$ as $\xi_4^k \triangleq (i^*, p^*, T_{i^*})$. Fulfilled if a communication chain by (3)

TABLE II
SUMMARY OF ONLINE OPERATOR-FLEET REQUESTS

Request	Type	Description and Notation
$\{\xi_1^k\}$	Operator-robot	Intra-team latency of team \mathcal{T}_k should be bounded by T_h^k .
$\{\xi_2^k\}$	Operator-robot	Regions \mathcal{P}^+ and \mathcal{P}^- should be prioritized/explored and avoided.
$\{\xi_3^k\}$	Operator-robot	Dynamic movement of operator h_k to the new location as $p_h^{k,*}$.
$\{\xi_4^k\}$	Operator-robot	Communication chain to robot i^* at p^* for time T_{i^*} .
$\{\xi_5^i\}$	Robot-operator	Data D_i should be modified by operator and returned as D_i^+ .
$\{\xi_6^i\}$	Robot-operator	Direct assistance to robot i at position p_i for duration T_i .
$\{\xi_7^{k_1 k_2}\}$	Op-operator	Inter-team latency of team \mathcal{T}_{k_1} and \mathcal{T}_{k_2} should be bounded by T_c .

is established from the operator to robot i^* via relays, and uninterrupted for duration T_{i^*} .

Robot-operator requests. Any robot can send two types of requests $\xi_{5,6}^i$ to the operators. (I) Confirmation and modification $\{\xi_5^i\}$. Robot i requests an immediate confirmation from any operator regarding actions and features, denoted by $\xi_5^i \triangleq D_i$. Fulfilled if D_i reaches any operator and is returned as modified data D_i^+ ; (II) Direct assistance $\{\xi_6^i\}$. Robot i requests assistance in unexpected situations $\xi_6^i \triangleq (p_i, T_i)$. Fulfilled if a communication chain is established from *any* operator to robot i at $p_i \in M_i$, uninterrupted for duration $T_i > 0$.

Operator-operator requests. Each operator h_{k_1} can send one type of request to another operator h_{k_2} , as the inter-team latency constraint $\{\xi_7^{k_1 k_2}\}$. One robot in team \mathcal{N}_{k_1} must communicate with one robot in team \mathcal{N}_{k_2} at least once every period of $T_c > 0$. This request remains active once issued.

Thus, the set of all requests received by $t \geq 0$ is denoted by $\Xi(t) \triangleq \{\{\xi_{1,2,3,4}^k\}, \{\xi_{5,6}^i\}, \{\xi_7^{k_1 k_2}\}\}$, which are unknown beforehand. Each request is removed from $\Xi(t)$ once fulfilled.

Remark 3. Both the intra-team latency $\{\xi_1^k\}$ and the inter-team latency $\{\xi_7^{k_1 k_2}\}$ are treated as online requests despite being perpetually active once issued. This is because both bounds as T_h^k and T_c can be modified online according to exploration progress, e.g., increased as subgroups move further away and the newly-explored area decreases. ■

D. Problem Statement

Consequently, the behavior of each robot or an operator can be described by a timed sequence of navigation and communication events as their local plans.

Definition 4. The *local plan* of robot $i \in \mathcal{N}$ is denoted by:

$$\Gamma_i \triangleq \tau_i^0 \mathbf{c}_i^0 \tau_i^1 \mathbf{c}_i^1 \tau_i^2 \mathbf{c}_i^2 \cdots, \quad (4)$$

where $\mathbf{c}_i^\ell \triangleq (p_i^\ell, i_i^\ell, D_i^\ell)$ is a communication event defined by the communication location, the other robot or the operator, and the exchanged data from (2); the navigation path $\tau_i^\ell \subset \mathcal{A}$ is the timed sequence of waypoints that robot i has visited between the consecutive communication events; and $\ell > 0$ records the round of communication events. ■

Note that the behavior of an operator h_k is defined similarly to Γ_k , for all $k \in \mathcal{K}$. For brevity, let $\hat{\Gamma} \triangleq \{\Gamma_i\} \cup \{\Gamma_k\}$ denote the joint plan of all robots and operators, and write $\hat{\Gamma} \models \Xi(t)$ if the behaviors of the multi-operator multi-robot system collectively fulfill the requirements of the requests in $\Xi(t)$. Accordingly, the overall mission-level objective can be stated as follows:

$$\begin{aligned} & \min_{\hat{\Gamma}, \bar{T}} \bar{T} \\ \text{s.t. } & \mathcal{A} \subseteq M_h^k(\bar{T}), \forall k, \\ & (1) - (4), \forall i, \forall k, \quad \hat{\Gamma} \models \xi, \forall \xi \in \Xi, \end{aligned} \quad (5a) \quad (5b)$$

where $\hat{\Gamma}$ is the joint plan of all robots and operators, and $\bar{T} > 0$ is the time instant when the environment is completely mapped and the resulting map is available to all operators, as required by (5a). Constraint (5b) enforces both the operational constraints and the fulfillment of all requests in Ξ .

Problem (5) defines the overall mission-level objective. In the online setting considered here, however, the request set is revealed incrementally during execution, and future operator motions, robot encounters, and communication opportunities are not known a priori. Therefore, MoRoCo does not solve (5) directly as a globally optimal planning problem. Instead, it realizes this mission objective through a sequence of online feasible coordination decisions on the current communication backbone, as detailed in Sec. IV-C.

Remark 4. The consideration of multiple teams, each with one operator and a few robots, is motivated by several practical concerns: (I) The workspace is large and complex, making it suitable for several medium-size fleets to explore in parallel; (II) One operator has limited attention to supervise and interact with too many robots, as revealed by several recent studies in [42], [44]; and (III) The response to online requests within one team is more efficient compared with a global team. More numerical comparisons can be found in the experiments. ■

IV. PROPOSED SOLUTION

As illustrated in Fig. 2, MoRoCo consists of three coupled components. Sec. IV-A presents the latency-bounded intermittent communication backbone and the detach-and-rejoin procedure for dynamic resizing. Then, Sec. IV-B introduces the request-consistent embedded-graph instantiation layer. Sec. IV-C presents the online coordination strategy for handling multiple simultaneous requests. Generalizations and limitations are discussed in Sec. IV-D.

A. Latency-bounded Intermittent Communication Protocol with Dynamic Resizing

Timely information sharing between the operators and the fleet is essential for online request handling. MoRoCo therefore first establishes a latency-bounded intermittent communication backbone on a joint-wheel graph, and augments it with a distributed detach-and-rejoin mechanism for dynamic resizing. Together, these components provide the backbone for the request-instantiation and online coordination layers.

1) *Latency-bounded Intermittent Communication Protocol:*

Consider a single team \mathcal{T} with the operator h and the robots \mathcal{N} , tasked with the information gathering tasks $\mathcal{F} \triangleq \{f_m\}$, where each task f_m specifies a location to be visited for information, such as exploration. The information collected by *any* robot i at time t must reach the operator within a predefined latency bound $T_h > 0$. Let $\delta_h(t) > 0$ denote the maximum latency over all the robots at time t .

Problem 1. Given the tasks \mathcal{F} and the bound T_h , synthesize the local plans $\{\Gamma_i\}$ such that the completion time of \mathcal{F} is minimized and the latency $\delta_h(t) \leq T_h$ holds for all $t > 0$. ■

The core idea is to enforce bounded latency through scheduled pairwise communication. The robots exchange the information at the communication events and replan the next event so that a timely return to the operator remains feasible within T_h . This logic is captured conveniently by an embedded joint-wheel coordination graph defined as follows.

Definition 5. An *embedded graph* is a tuple $\mathcal{G} \triangleq (\mathcal{V}, \mathcal{E}, \sigma, x)$, where \mathcal{V} is the vertex set; $\mathcal{E} \subseteq \mathcal{V} \times \mathcal{V}$ is the edge set; $\sigma \triangleq (\sigma_{\mathcal{V}}, \sigma_{\mathcal{E}})$ embeds vertex and edge into attributes $(\Sigma_{\mathcal{V}}, \Sigma_{\mathcal{E}})$; and $x: \mathcal{V} \rightarrow \mathbf{X}_{\mathcal{V}}$ is the geometric embedding. ■

Definition 6. An *embedded joint-wheel coordination graph* is an embedded graph $\mathcal{G}^w \triangleq (\mathcal{V}, \mathcal{E}, \sigma, x)$ such that: (I) $\mathcal{V} \triangleq \mathcal{N} \cup \{h\}$; (II) $\mathcal{E} \triangleq \mathcal{E}_r \cup \mathcal{E}_h$, where \mathcal{E}_r forms a ring over \mathcal{N} , i.e., $(k_\ell, k_{\ell+1}) \in \mathcal{E}_r$ for $\ell = 1, \dots, N$ with $k_{N+1} \triangleq k_1$, and $\mathcal{E}_h \triangleq \{(h, i) \mid i \in \mathcal{N}\}$. ■

Remark 5. As illustrated in Fig. 4, the term *joint-wheel* emphasizes a joint connectivity rather than a static graph. At any time instant, the communication protocol activates at most one rim edge in \mathcal{E}_r , hence only one robot pair communicates. Over a period longer than T_h , the union of all rim edges in \mathcal{E}_r and hub edges in \mathcal{E}_h induces a wheel-like connectivity pattern. This should be distinguished from the static line and star graphs introduced later. ■

The embedded graph \mathcal{G}^w above is constructed and maintained in a fully distributed way via local coordination at intermittent communication events as described below.

Initialization. To begin with, the vertex embedding encodes the local coordination state, defined as:

$$\sigma_{\mathcal{V}}(i) \triangleq (\Gamma_i, \chi_i), \quad \sigma_{\mathcal{V}}(h) \triangleq (\hat{p}_h, \chi_h), \quad (6)$$

where the local plan Γ_i specifies the sequence of visiting locations and communication events for robot i as in (4); the latency variable $\chi_i \in \mathbb{R}^N$ estimates the minimum time stamp of information from each robot that is guaranteed to reach the operator; and $\hat{p}_h \in \mathbb{R}^2$ is the current target location of the operator, while $\chi_h \in \mathbb{R}^N$ is the confirmed time stamp of each robot. The initialization assigns $\Gamma_i = \emptyset$ and $\chi_i = \mathbf{0}$ for all $i \in \mathcal{N}$, with $\hat{p}_h = \emptyset$ and $\chi_h = \mathbf{0}$. Moreover, the edge embedding encodes the scheduled communication events as:

$$\sigma_{\mathcal{E}}(i, j) \triangleq (t_{ij}^+, p_{ij}^+), \quad \forall (i, j) \in \mathcal{E}_r; \quad (7)$$

and $\sigma_{\mathcal{E}}(h, i) \triangleq (t_{hi}^+, p_{hi}^+)$ are similar for each $i \in \mathcal{N}$. The initial communications are set to $\sigma_{\mathcal{E}}(i, j) = (0, p_h)$, as all robots start around the operator location and communicate

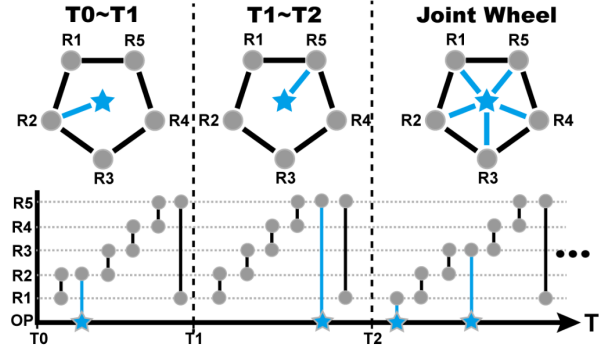


Fig. 4. **Top:** the joint-wheel communication graph over time; **Bottom:** the pairwise meeting events (black vertical lines) and return events (blue lines).

immediately. The value $\sigma_{\mathcal{E}}(h, i) = \emptyset$ indicates that no return is scheduled initially. Lastly, the geometric embedding assigns each vertex its physical state and its local data, written as $x(i) \triangleq (p_i(t), D_i(t))$ and $x(h) \triangleq (p_h(t), D_h(t))$.

Pairwise Coordination. At a communication event c_{ij} , the robots read the current geometric states $x(i)$ and $x(j)$, exchange the incident embeddings, and compute the fused map \mathcal{M}_{ij} . The exchange yields the merged latency vector:

$$\chi_{ij} \triangleq \mathbf{max}\{\chi_i, \chi_j\}, \quad (8)$$

where the maximum operation is taken component-wise. Then, the coordination computation proceeds in three stages, as summarized in Alg. 1 and Fig. 5.

Stage-I: Determine Return Event. The quantity $\underline{\chi}_{ij} \triangleq \min_{k \in \mathcal{N}} \{\chi_{ij}(k)\}$, is the minimum team time stamp that is guaranteed to reach the operator, as inferred at c_{ij} . Let $t_\ell^{L\ell}$ and $p_\ell^{L\ell}$ denote the terminal time and location in the local plan Γ_ℓ of robot $\ell \in \{i, j\}$. The earliest arrival time at the operator for a candidate return robot $\ell \in \{i, j\}$ is estimated as:

$$t_{h\ell}^* \triangleq t_\ell^{L\ell} + T_\ell^{\text{nav}}(p_\ell^{L\ell}, \hat{p}_h), \quad (9)$$

where $T_\ell^{\text{nav}}(\cdot, \cdot)$ is the navigation-time model and the detailed construction is provided in the Supplementary file. A return to the operator is unnecessary if:

$$\min_{\ell \in \{i, j\}} \{t_{h\ell}^*\} \leq (T_h + \underline{\chi}_{ij}), \quad (10)$$

and otherwise the return robot is selected as $n \triangleq \mathbf{argmin}_{\ell \in \{i, j\}} \{t_{h\ell}^*\}$, where n denotes the robot that returns to the operator immediately after its last event.

Stage-II: Optimize Task Sequence and Next Communication Event. Conditioned on the return decision, the optimization produces the tailing plans for both robots: $\Gamma_i^+ \triangleq \tau_i^+ \mathbf{c}_{ij}^+$ and $\Gamma_j^+ \triangleq \tau_j^+ \mathbf{c}_{ij}^+$, where τ_i^+ and τ_j^+ are the optimized task sequences and \mathbf{c}_{ij}^+ is the next communication event shared by the two robots. The schedule of \mathbf{c}_{ij}^+ is set to (t_{ij}^+, p_{ij}^+) , which is constrained locally due to the latency bound:

$$t_{ij}^+ + T_\ell^{\text{nav}}(p_{ij}^+, \hat{p}_h) \leq T_h + \chi^*, \quad (11)$$

where $\chi^* \triangleq \underline{\chi}_{ij}$ if no return is scheduled in Stage-I, and χ^* is computed using the scheduled return otherwise. Feasible outputs $(\tau_i^+, \tau_j^+, \mathbf{c}_{ij}^+)$ are obtained by an iterative TSP-based procedure. At each iteration, a TSP is constructed over the remaining task locations in \mathcal{F}^- together with the current

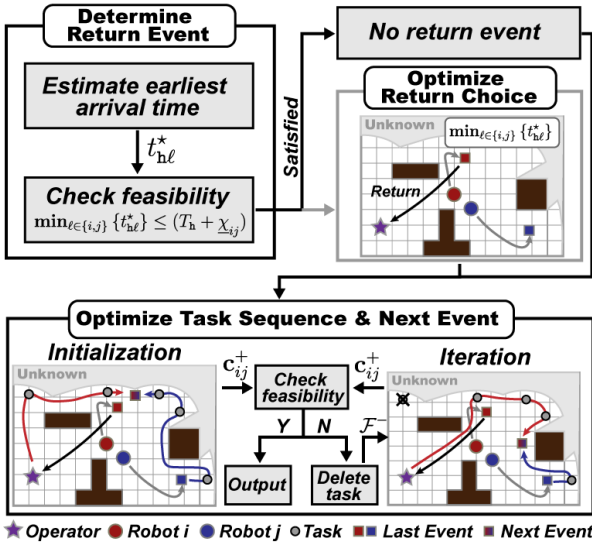


Fig. 5. The proposed pairwise coordination scheme via intermittent communication. **Top**: return event to the operator is determined first; **Bottom**: the next meeting event is optimized given the current exploration tasks.

terminal locations of robots i and j . The edge weights are given by the navigation time model $T^{\text{nav}}(\cdot)$. The TSP solution yields a joint visiting order \mathbf{p}_{ij} , from which τ_i^+ and τ_j^+ are extracted, and a candidate \mathbf{c}_{ij}^+ is selected along \mathbf{p}_{ij} . Feasibility of the meeting event is checked by (11). If violated, a task in τ_i^+ or τ_j^+ is removed and the procedure repeats.

Stage-III: Update Embeddings. Consequently, the current event \mathbf{c}_{ij} is removed from the plans to obtain the prefixes Γ_i^- and Γ_j^- . The updated plans satisfy $\hat{\Gamma}_i = \Gamma_i^- \Gamma_i^+$ and $\hat{\Gamma}_j = \Gamma_j^- \Gamma_j^+$. The latency vectors are updated by the information exchange as $\hat{\chi}_i \triangleq \hat{\chi}_j \triangleq \chi_{ij}$, where χ_{ij} is defined in (8). The local embedding update is then given by:

$$\begin{aligned} \sigma_V(i) &\leftarrow (\hat{\Gamma}_i, \hat{\chi}_i), & \sigma_V(j) &\leftarrow (\hat{\Gamma}_j, \hat{\chi}_j); \\ \sigma_E(i, j) &\leftarrow (t_{ij}^+, p_{ij}^+), & \sigma_E(h, n) &\leftarrow (t_{hn}^*, \hat{p}_h); \end{aligned} \quad (12)$$

where the last line is applied only if Stage-I schedules a return, and the hub-edge embedding remains \emptyset otherwise.

Combined with the joint-wheel communication topology, the above procedure ensures exploration with bounded latency, as shown in the following lemmas and theorem. The detailed proofs are provided in the Appendix.

Lemma 1. *The latency constraint $\delta_h(t) \leq T_h, \forall t > 0$ is satisfied if for every return event $\mathbf{c}_{h, n_i} \in \Gamma_h$, it holds that: (I) $t_h(n_i) \leq T_h + \chi_{n_{i-1}}$ and (II) $\chi_{n_i} > \chi_{n_{i-1}}$.*

Lemma 2. *The iteration process in Alg. 1 ends in finite steps, and always returns a feasible plan that satisfies the meeting event constraint (11) during each pairwise coordination.*

Theorem 1. *Under the joint-wheel communication topology and the coordination protocol in Alg. 1, the intra-team latency constraint is satisfied, i.e., $\delta_h(t) \leq T_h$ holds for all $t > 0$.*

Remark 6. The joint-wheel graph above typically consists of at least three robots. For $|\mathcal{N}| = 1$, the robot explores independently and returns to the operator periodically by T_h^k . For $|\mathcal{N}| = 2$, the same protocol is applied on a line topology and the local plan reduces to $\Gamma_i \triangleq \tau_i \mathbf{c}_i$. ■

Algorithm 1: Latency-aware Intermittent Pair-wise Coordination: PairCoord(\cdot)

Input : Local plans Γ_i, Γ_j , Stamp χ_{ij} , Map \mathcal{M}_{ij} , Unassigned tasks \mathcal{F}^- .

Output: Revised local plans $\hat{\Gamma}_i, \hat{\Gamma}_j$; next event \mathbf{c}_{ij}
 /* **Determine Return Event.** */

- 1 Compute $t_{h\ell}^*$ by (9) for $\ell \in \{i, j\}$;
 - 2 **if** condition (10) **not** satisfied **then**
 - 3 Determine return robot by $n \triangleq \operatorname{argmin}_{\ell \in \{i, j\}} \{t_{h\ell}^*\}$;
 - 4 Append a return event to Γ_n ;
 - /* **Optimize Task Sequence and Next Pairing Event.** */
 - 5 $\mathbf{p}_{ij} \leftarrow \text{TSP-Path}(p_i^{L_i}, \mathcal{F}^-, p_j^{L_j})$;
 - 6 $\mathbf{c}_{ij} \leftarrow \text{SelComm}(\mathbf{c}_i^{L_i}, \mathbf{c}_j^{L_j}, \mathbf{p}_{ij})$;
 - 7 **while** condition (11) **not** satisfied **do**
 - 8 Remove f^* with maximum cost from \mathcal{F}^- ;
 - 9 Recompute \mathbf{p}_{ij} and \mathbf{c}_{ij} ;
 - 10 $\tau_i^+, \tau_j^+ \leftarrow \text{Split}(\mathbf{p}_{ij}, \mathbf{c}_{ij})$;
 - /* **Update Local Plans.** */
 - 11 $\Gamma_\ell^- \leftarrow \text{Remove}(\Gamma_\ell, \mathbf{c}_{ij})$, for $\ell \in \{i, j\}$;
 - 12 $\hat{\Gamma}_\ell \leftarrow \Gamma_\ell^- + \tau_\ell^+ + \mathbf{c}_{ij}$, for $\ell \in \{i, j\}$;
 - 13 Update embeddings via (12);
-

2) *Distributed Detach-and-Rejoin Mechanism:* Flexible re-sizing under intermittent communication is enabled through a distributed detach-and-rejoin procedure that preserves the wheel topology and respects latency constraints. A central design choice is to complete rewiring through *two consecutive meeting events*, ensuring that successor robots receive consistent plan and adjacency updates before a robot leaves or rejoins the wheel, which is illustrated in Fig. 6.

(I) **To detach**, consider three consecutive robots (i, j, k) along the wheel, where robot j intends to detach. Let Γ_ℓ denote robot ℓ 's nominal local plan and $\hat{\Gamma}_\ell$ the optimized plan maintained online. At the meeting between robots i and j , robot j does not depart immediately. Instead, using robot i 's most recent knowledge of robot k 's plan Γ_k , robot i computes a bypass schedule that directly connects (i, k) , via $\hat{\Gamma}_i, \hat{\Gamma}_k, \mathbf{c}_{ik} = \text{PairCoord}(\Gamma_i, \Gamma_k)$; and updates the edge embeddings by removing (i, j) and inserting (i, k) , i.e.,

$$\sigma_E(i, j) \leftarrow \emptyset, \quad \sigma_E(i, k) \leftarrow (t_{ik}, p_{ik}),$$

where (t_{ik}, p_{ik}) is the time–location pair of the next event \mathbf{c}_{ik} . Robot j then follows its original schedule to meet robot k and forwards the bypass message so that robot k adopts $\hat{\Gamma}_k$ and records the updated predecessor implied by \mathbf{c}_{ik} . Only after this second meeting does robot j finalize detachment and depart to remote location. Thus, the detach event is denoted by:

$$\pi_j \triangleq (j, t_{jk}, p_{jk}), \quad (13)$$

where (t_{jk}, p_{jk}) is the confirmed meeting between (j, k) as the time and location for robot j to detach from \mathcal{G}_k .

(II) **To rejoin**, robot j first returns to the operator h and waits until a team robot m also arrives at h . Reinsertion is completed by two consecutive meetings. Let ℓ denote robot m 's current successor on the wheel. First,

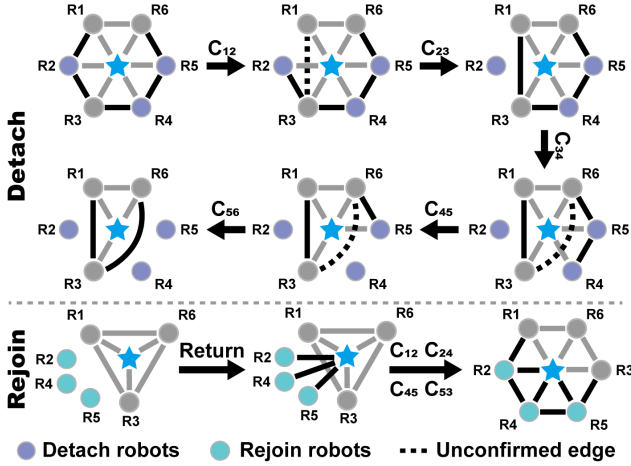


Fig. 6. The distributed schemes of detach (**Top**) and rejoin (**Bottom**), where the edges can be involved (black), unrelated (gray), and unconfirmed (dashed).

robots m and j execute pair-wise coordination at h to synchronize plans and schedule the next event as $\hat{\Gamma}_m, \hat{\Gamma}_j, c_{mj} = \text{PairCoord}(\Gamma_m, \Gamma_j)$. Then, the embeddings are updated by replacing the successor edge (m, ℓ) with (m, j) , i.e.,

$$\sigma_{\mathcal{E}}(m, \ell) \leftarrow \emptyset, \quad \sigma_{\mathcal{E}}(m, j) \leftarrow (t_{mj}, p_{mj}),$$

where (t_{mj}, p_{mj}) is from event c_{mj} . Second, robot j meets robot ℓ to establish the new successor relation via $\text{PairCoord}(\Gamma_j, \Gamma_{\ell})$, and the edge embedding $\sigma_{\mathcal{E}}(j, \ell) \leftarrow (t_{j\ell}, p_{j\ell})$ is added. This two-step reinsertion avoids inconsistent topology and restores a valid wheel graph.

Lastly, for *multiple* detaching or rejoining robots, the above scheme can be extended by adjusting the number of required forwarding meetings. For detachment, nonconsecutive robots may detach sequentially using the same two-meeting handoff. If a consecutive block detaches, a single bypass plan is computed by the predecessor of the block and is forwarded across the block until reaching the first non-detaching successor; each intermediate robot forwards once and then exits. For rejoining, a block waiting at the operator h can be inserted between a returning robot m and its successor through consecutive pairwise coordination; the last inserted robot then performs the successor take-over meeting to close the wheel.

B. Request-consistent Embedded Graph Instantiation

Built on the latency-bounded communication, this section presents the request-instantiation layer of MoRoCo. Given the wheel backbone and an incoming request, it constructs a request-consistent embedded graph together with the resized backbone and the detach schedule. It then introduces the procedure to compute this transition, followed by the request-specific graph constructions and detach-rejoin executions.

1) Problem of Request-consistent Graph Instantiation:

Within MoRoCo, each request ξ in Table II is realized through a family of candidate embedded target graphs that encode the desired robot roles and communication topology, denoted by $\hat{\mathcal{G}}_k^{\xi}$. Given the current embedded wheel backbone graph \mathcal{G}_k^w , the request-instantiation problem seeks: a resized wheel backbone $\mathcal{G}_k^{w'}$, a selected target graph $\mathcal{G}_k^{\xi} \in \hat{\mathcal{G}}_k^{\xi}$, and the cor-

Algorithm 2: Request-consistent graph instantiation for a given request $\text{GraphMatch}(\cdot)$

Input : \mathcal{G}_k^w , request ξ , candidate set $\hat{\mathcal{G}}_k^{\xi}$, weight w_n

Output: $\mathcal{G}_k^{\xi}, \mathcal{G}_k^{w'}, \hat{\pi}_r^{\xi}, \Pi_k^{\xi}$

- 1 Extract \mathcal{C}_k^+ from \mathcal{G}_k^w ;
 - 2 **while** candidates in $\hat{\mathcal{G}}_k^{\xi}$ remain **do**
 - 3 Select candidate graph \mathcal{G}_k^{ξ} given $\mathcal{C}_k^+, \mathbf{p}_0^{\xi}$ by (18);
 - 4 Extract $\mathcal{N}_k^{\xi}, \mathbf{p}_0^{\xi}$ from \mathcal{G}_k^{ξ} ;
 - 5 $\mathcal{G}_k^{w'} \leftarrow \mathcal{G}_k^w[\mathcal{N}_k \setminus \mathcal{N}_k^{\xi}]$;
 - 6 $(T_{\text{trs}}, \hat{\pi}_r^{\xi}) \leftarrow \text{MultiDetach}(\mathcal{G}_k^w, \mathcal{N}_k^{\xi})$ by (16);
 - 7 $\Pi_k^{\xi} \leftarrow \text{LBAP}(\mathcal{N}_k^{\xi}, \mathbf{p}_0^{\xi}, \hat{\pi}_r^{\xi})$ by (17);
 - 8 Update best $\hat{\mathcal{G}}_k^{\xi}$ by (14);
 - 9 **return** $\mathcal{G}_k^{\xi}, \mathcal{G}_k^{w'}, \hat{\pi}_r^{\xi}, \Pi_k^{\xi}$ with the best candidate;
-

responding detach events $\hat{\pi}_k^{\xi} \triangleq \{\pi_r^{\xi}\}$ that realize the required topology transition. The performance measure is given by:

$$\min_{\mathcal{G}_k^{w'}, \mathcal{G}_k^{\xi}, \hat{\pi}_k^{\xi}, \Pi_k^{\xi}} \left(T_k^{\text{trs}}(\mathcal{G}_k^w, \mathcal{G}_k^{w'}) + w_n \max_{r \in \mathcal{N}_k^{\xi}} \left\{ T_r^{\text{nav}}(\pi_r^{\xi}, \Pi_k^{\xi}) \right\} \right), \quad (14)$$

where $T_k^{\text{trs}}(\mathcal{G}_k^w, \mathcal{G}_k^{w'})$ is the transition time induced by resizing the wheel backbone; $T_r^{\text{nav}}(\pi_r^{\xi}, \Pi_k^{\xi})$ is the navigation time for robot r to execute its detach event and reach the role specified by the assignment Π_k^{ξ} ; \mathcal{N}_k^{ξ} is the set of robots that switch from \mathcal{G}_k^w to \mathcal{G}_k^{ξ} ; and $w_n > 0$ trades off the backbone-transition time and the request-realization time.

Problem 2. Given the current wheel backbone graph \mathcal{G}_k^w and the candidate target graphs $\hat{\mathcal{G}}_k^{\xi}$ for request ξ , define a graph instantiation procedure:

$$\mathcal{G}_k^{w'}, \mathcal{G}_k^{\xi}, \hat{\pi}_k^{\xi}, \Pi_k^{\xi} = \text{GraphMatch}(\mathcal{G}_k^w, \hat{\mathcal{G}}_k^{\xi}, \xi), \quad (15)$$

which realizes a request-consistent topology transition by minimizing the objective in (14). ■

2) *Optimization Procedure:* As illustrated in Fig. 7, given a request-induced candidate set $\hat{\mathcal{G}}_k^{\xi}$, it first computes a feasible transition schedule to resize the wheel backbone, then assigns detached robots to target roles through an unbalanced linear bottleneck assignment, and finally traverses the candidate set to return the solution that minimizes (14).

The first step evaluates the transition time required to resize the current wheel backbone into a feasible smaller wheel. For a candidate $\mathcal{G}_k^{\xi} \in \hat{\mathcal{G}}_k^{\xi}$, let \mathcal{N}_k^{ξ} denote the robots allocated to \mathcal{G}_k^{ξ} . Removing \mathcal{N}_k^{ξ} from the wheel backbone \mathcal{G}_k^w yields the resized wheel $\mathcal{G}_k^{w'}$. Conditioned on the return robot that conveys the request, the detachment routine in Sec. IV-A2 is invoked to produce a feasible timed schedule and its transition time:

$$(T_{\text{trs}}(\mathcal{G}_k^w, \mathcal{G}_k^{w'}), \hat{\pi}_r^{\xi}) \triangleq \text{MultiDetach}(\mathcal{G}_k^w, \mathcal{N}_k^{\xi}), \quad (16)$$

where each $\hat{\pi}_r^{\xi} \triangleq (r, t_r, p_r)$ specifies the detach time and detach location of robot r . The transition completion time T_{trs} is the earliest time when $\mathcal{G}_k^{w'}$ is fully formed and its embeddings are updated by (12).

In the second step, the detached robots are assigned to the role locations of the selected target graph \mathcal{G}_k^{ξ} . Let $\mathbf{p}_0^{\xi} \triangleq$

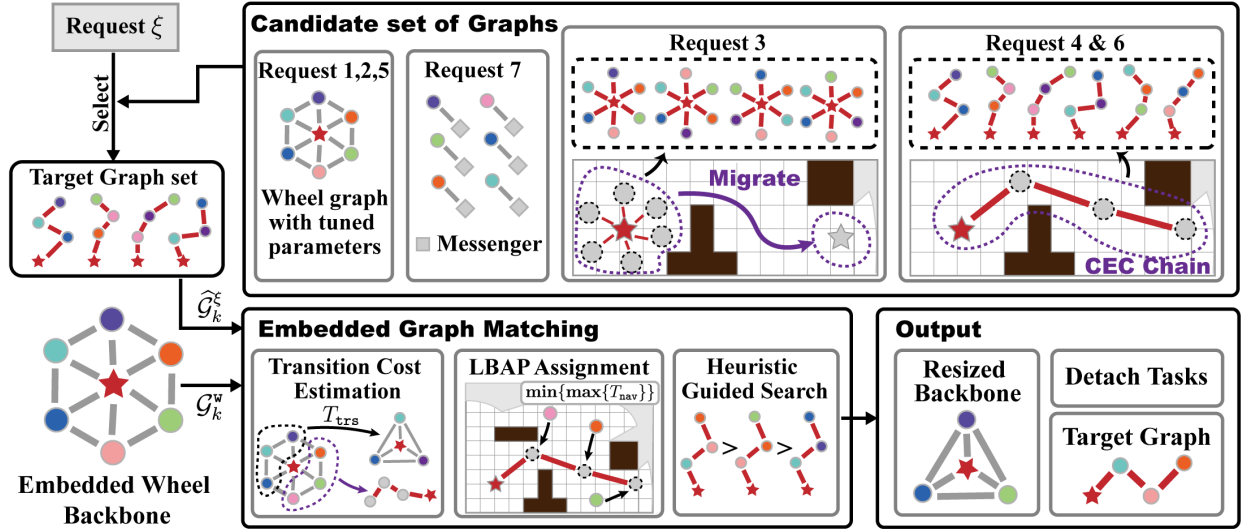


Fig. 7. Illustration of the request-consistent graph instantiation procedure. Given a request ξ , GraphMatch selects a request-specific target graph from a candidate set and realizes it from the embedded wheel backbone \mathcal{G}_k^w , yielding a resized backbone, the instantiated target graph, and the detach events.

$\{p_r^\xi\}_{r \in \mathcal{N}_k^\xi}$ be the initial role locations in \mathcal{G}_k^ξ . An assignment $\Pi_k^\xi : \mathcal{N}_k^\xi \rightarrow \mathbf{p}_0^\xi$ induces the bottleneck arrival time $\max_{r \in \mathcal{N}_k^\xi} \{t_r + T_{\text{nav}}^r(p_r, \Pi_k^\xi(r))\}$, where $T_{\text{nav}}^r(p_r, \Pi_k^\xi(r))$ is the navigation time from the detach location to the assigned role. Selecting Π_k^ξ to minimize this term yields an unbalanced linear bottleneck assignment problem (LBAP) [47]:

$$\Pi_k^\xi \leftarrow \text{LBAP}(\mathcal{N}_k^\xi, \mathbf{p}_0^\xi, \hat{\pi}_r^\xi), \quad (17)$$

which can be solved efficiently by off-the-shelf tools such as OR-Tools [48], and returns a concrete role assignment and the navigation plans for all detached robots.

The final step traverses the candidate set $\hat{\mathcal{G}}_k^\xi$ using a best-first heuristic. After evaluating the current candidate $\mathcal{G}_{k,q}^\xi$, the next candidate is selected by ranking the remaining graphs via the surrogate score below, derived from (14):

$$\mathcal{G}_{k,q+1}^\xi = \underset{\mathcal{G} \in \hat{\mathcal{G}}_k^\xi \setminus \{\mathcal{G}_{k,q}^\xi\}}{\text{argmin}} (\tilde{T}_k^{\text{trs}}(\mathcal{G}, \mathcal{C}_k^+) + w_n \tilde{T}_k^{\text{nav}}(\mathbf{p}_0^\xi, \mathcal{C}_k^+)), \quad (18)$$

where \mathcal{C}_k^+ is the set of subsequent meeting events to be executed as implied by the local plans $\{\Gamma_i\}$. Here $\tilde{T}_k^{\text{trs}}(\mathcal{G}, \mathcal{C}_k^+)$ and $\tilde{T}_k^{\text{nav}}(\mathbf{p}_0^\xi, \mathcal{C}_k^+)$ are fast predictors of the transition completion time and bottleneck arrival time, respectively, conditioned on the confirmed meeting events \mathcal{C}_k^+ . This heuristic prioritizes candidates that are likely to admit early feasible detachment and short worst-case travel, while avoiding repeated evaluation of exact durations during the search. The overall realization procedure is summarized in Alg. 2. Its role within MoRoCo is to return an executable request-consistent transition for a given candidate family, as formalized by the following lemma and its proof provided in the Appendix.

Lemma 3. *For any request ξ for team \mathcal{T}_k , suppose there exists at least one candidate $\mathcal{G}_k^\xi \in \hat{\mathcal{G}}_k^\xi$ such that (16) returns a detach schedule for the associated robot set \mathcal{N}_k^ξ . Then Alg. 2 terminates in finite time and returns $(\mathcal{G}_k^{w'}, \mathcal{G}_k^\xi, \hat{\pi}_k^\xi)$, together with Π_k^ξ , such that the resulting transition is executable under the detach mechanism and the objective in (14) is minimized over all candidates in $\hat{\mathcal{G}}_k^\xi$.*

3) *Request-Specific Execution Modes:* Requests are executed either by updating the embeddings of the wheel backbone or by instantiating a request-specific embedded subgraph through the detach–execute–rejoin mechanism. When a request requires a topology transition, Alg. 2 is invoked to instantiate a feasible target subgraph and return role assignments together with timed detach events for the involved robots, while the remaining robots preserve the wheel backbone to maintain latency-bounded intermittent communication.

(I) **Intra-team communication with bounded latency.** For intra-team exploration requests ξ_1^k , ξ_2^k , and ξ_5^k , the joint-wheel backbone \mathcal{G}_k^w is retained and no subgraph instantiation is required. The base request ξ_1^k is satisfied directly by the backbone, which enforces the latency-bounded information flow. Requests ξ_2^k and ξ_5^k are realized by modifying the embeddings in (12) under the same topology. Specifically, ξ_2^k excludes frontiers inside the prohibited region \mathcal{P}^- and prioritizes other frontiers toward \mathcal{P}^+ via the embedded weights:

$$J(f) \triangleq \sum_{p \in \mathcal{P}^+} \|x(f) - p\|, \quad \forall f \in \mathcal{F}_k, \quad (19)$$

such that larger $J(f)$ is deprioritized. Request ξ_5^k appends an immediate return opportunity for timely delivery of D_i , updating the relevant time-stamps in the embeddings without changing \mathcal{G}_k^w for the remaining period.

(II) **Inter-team exchange with bounded latency.** For the inter-team request $\xi_7^{k_1 k_2}$, neighboring teams \mathcal{T}_{k_1} and \mathcal{T}_{k_2} periodically exchange compressed mission data under the inter-team bound T_c . This request is realized as a singleton messenger subgraph, where a messenger robot detaches from its backbone, reaches an external meeting event $\mathbf{c}_e = (p_e, t_e)$, exchanges data, and rejoins. Feasibility with respect to the intra-team meeting sequence is enforced by selecting a messenger robot from the most recent intra-team meeting pair and scheduling the external event according to:

$$t_{ij}^+ + T_\ell^{\text{nav}} \geq t_e, \quad \forall \ell \in \{i, j\},$$

$$p_e^+ = \underset{p \in \tau_{k_1 k_2}}{\text{argmin}} \left\{ \max_{\ell = k_1, k_2} \left\{ T_{m_\ell}^{\text{nav}}(p_{n_\ell}, p) \right\} \right\}, \quad (20)$$

Algorithm 3: Overall online execution of the MoRoCo framework $\text{MoRoCo}(\cdot)$

Input : $\{\mathcal{G}_{k,0}^w\}, \{\Gamma_i\}$.
Output: Local plans $\{\Gamma_i\}$ and evolving graphs $\{\mathcal{G}_k\}$.

```

1 while not terminated and all teams  $\{\mathcal{T}_k\}$  in parallel do
  /* Within the wheel graph */
2  Robot  $i \in \mathcal{N}_k^w$  executes  $\Gamma_i$  in parallel;
3  if meeting event  $c_{ij}$  occurs then
4     $\Gamma_i, \Gamma_j, c_{ij}^+ \leftarrow \text{PairCoord}(\Gamma_i, \Gamma_j, \chi_{ij})$ ;
5    Update embeddings of  $\mathcal{G}_k^w$ ;
  /* Request instantiation */
6  if request bundle  $\Xi_k$  received then
7    Order requests in  $\Xi_k$  by priority;
8    foreach request  $\xi_k^\ell \in \Xi_k$  do
9      if  $\xi_k^\ell$  admissible on  $\mathcal{G}_k^w$  then
10        $\tilde{\mathcal{G}}_k^w, \tilde{\mathcal{G}}_k^\ell, \tilde{\pi}_k^\ell, \tilde{\Pi}_k^\ell \leftarrow$ 
11         GraphMatch( $\mathcal{G}_k^w, \tilde{\mathcal{G}}_k^\ell, \xi_k^\ell$ );
12       if an executable instantiation then
13          $\mathcal{G}_k^w \leftarrow \tilde{\mathcal{G}}_k^w$ , add  $\tilde{\mathcal{G}}_k^\ell$  to  $\mathcal{G}_k$ ;
14         Store  $\tilde{\pi}_k^\ell$  for detachment;
15     Follow detach schedules and update  $\mathcal{G}_k$ ;
  /* Request execution */
16  foreach active request  $\xi_k^\ell$  in parallel do
17    All robots in  $\mathcal{N}_k^\ell$  perform request  $\xi_k^\ell$ ;
18    if request  $\xi_k^\ell$  is fulfilled then
19      Trigger rejoin procedure and update  $\mathcal{G}_k$ ;

```

distributed and driven by local pairwise coordination in Alg. 1. Each team maintains an embedded communication graph \mathcal{G}_k , initialized as a joint-wheel backbone $\mathcal{G}_k = \mathcal{G}_{k,0}^w$ to satisfy the intra-team latency bound T_h^k specified by ξ_1^k , while inter-team exchanges under $\{\xi_7^{k_1 k_2}\}$ are constrained by the bound T_c . During robot meetings, local embeddings and data are updated and fused through $\text{PairCoord}(\cdot)$, enabling latency-bounded information propagation without centralized synchronization.

Upon receiving a new bundle Ξ_k , the online coordination layer of MoRoCo processes the requests sequentially under the admissibility condition (24), and instantiates executable request subgraphs within the overall runtime summarized in Alg. 3. Consequently, \mathcal{G}_k evolves into the union of the wheel backbone and the subgraphs required by active requests, such as a singleton for $\{\xi_7^{k_1 k_2}\}$, a line for $\{\xi_4^k\}$ and $\{\xi_6^k\}$, and a star for $\{\xi_3^k\}$. Robots detach to execute within the instantiated subgraphs, while the remaining wheel backbone continues exploration and preserves latency-bounded intermittent connectivity. After a request is completed, the corresponding subgraph is removed and the involved robots rejoin the backbone, restoring \mathcal{G}_k for continued exploration and subsequent online requests. The following theorem states the framework-level guarantee provided by the online execution policy in Alg. 3, with the proof provided in the Appendix.

Theorem 2. For any team \mathcal{T}_k and any finite-time arrival sequence of request bundles, suppose that whenever a request ξ_k^ℓ becomes admissible under the compatibility condition in (24), there exists at least one candidate $\mathcal{G}_k^{\xi_k^\ell} \in \tilde{\mathcal{G}}_k^{\xi_k^\ell}$ such that (16) re-

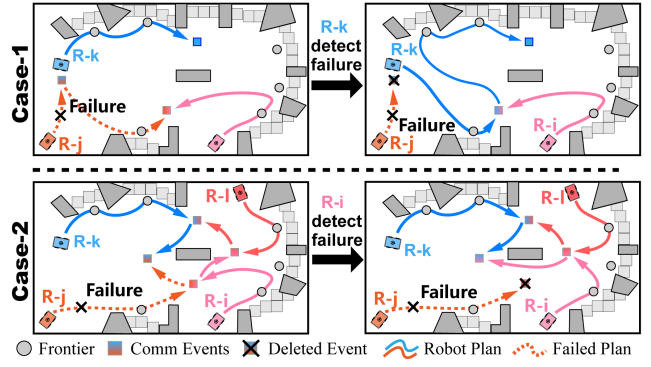


Fig. 9. The proposed failure detection and recovery scheme. **Top:** if robot j fails before meeting its predecessor k , robot k bypasses j after waiting T_{\max}^- ; **Bottom:** if j fails after meeting its successor i , robot i triggers recovery after waiting T_{\max}^+ , and the joint wheel topology is restored after two meetings.

turns a detach schedule for the associated robots $\mathcal{N}_k^{\xi_k^\ell}$. Assume further that every instantiated request subgraph completes its assigned request and rejoins the wheel backbone in finite time. Then Alg. 3 satisfies the following properties:

- (I) after each request activation or completion, the embedded graph $\mathcal{G}_k(t)$ remains an executable decomposition of the form (23), consisting of a remaining wheel backbone and finitely many subgraphs for active requests;
- (II) every request that becomes admissible and is instantiated by Alg. 3 is serviced in finite time;
- (III) there exists a finite time t_f such that $\mathcal{G}_k(t) = \mathcal{G}_k^w$ for all $t \geq t_f$, i.e., all request subgraphs have been removed and the complete wheel backbone is restored.

D. Discussion

1) *Complexity Analysis:* The computational cost of MoRoCo is event-driven. At robot meeting events, the dominant routine is $\text{PairCoord}(\cdot)$ in Alg. 1, whose cost is dominated by a TSP-path computation over the merged frontier set \mathcal{F}_{ij} with complexity $\mathcal{O}(|\mathcal{F}_{ij}|^3)$ and one shortest-path query on the explored map with complexity $\mathcal{O}(N_m \log N_m)$, yielding $\mathcal{O}(|\mathcal{F}_{ij}|^3(|\mathcal{F}_{ij}| + N_m \log N_m))$ overall, where \mathcal{F}_{ij} is the merged frontier set, and N_m is the number of map nodes. When topology instantiation is required, MoRoCo invokes $\text{GraphMatch}(\cdot)$, whose dominant step is the bottleneck assignment with complexity $\mathcal{O}(N_k^3)$, so the overall cost is $\mathcal{O}(N_c N_k^3)$, where N_c is the number of candidate graphs in $\tilde{\mathcal{G}}_k^\xi$ and N_k is the team size. Hence, for one request bundle $\Xi_k = \{\xi_k^\ell\}_{\ell=1}^L$, the online framework in Alg. 3 incurs the same cost as $\text{PairCoord}(\cdot)$ at meeting events, and otherwise processes admissible requests sequentially with complexity $\mathcal{O}\left(\sum_{\ell=1}^{L_a} N_{c,\ell} (N_k^{w,\ell-1})^3\right)$, where $L_a \leq L$ is the number of admissible requests; $N_{c,\ell}$ is the number of candidate graphs for ξ_k^ℓ ; and $N_k^{w,\ell-1}$ is the size of the remaining wheel backbone before the ℓ -th instantiation. Since $N_k^{w,\ell-1} \leq N_k$, this yields the worst-case bound $\mathcal{O}(L_a N_{c,\max} N_k^3)$, where $N_{c,\max} = \max_{\ell} \{N_{c,\ell}\}$. Hence, the online cost of MoRoCo scales linearly with the number of admissible requests in a bundle and cubically with the team size in the worst case.

2) *Generalization:* Several nontrivial extensions arise naturally from the MoRoCo framework, as validated in the sequel.

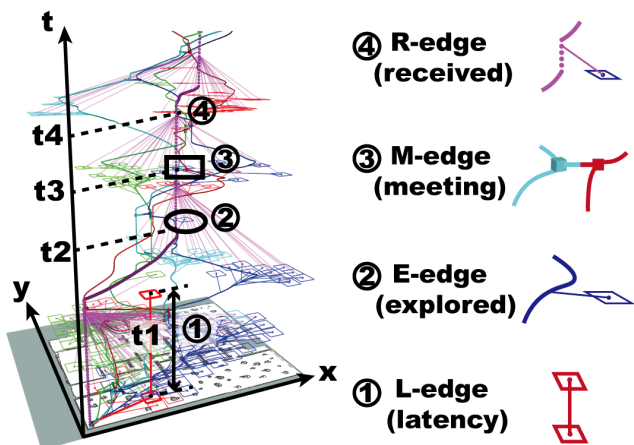


Fig. 10. **Left:** the proposed data structure as the spatial-temporal tree of data flow (*SDF-Tree*), to encapsulate information gathered during exploration and data-propagation; **Right:** the spatial-temporal trajectories of each robot and the operator, and four types of edges in the tree. Note that t_1 is the maximum latency, t_2 is the time of exploration for the grid area, t_3 is meeting time, and t_4 the time that this area is first received by operator.

(I) *Heterogeneous fleets.* Heterogeneity is handled by incorporating mobility and resource feasibility into navigation-time estimation, restricting goal selections to reachable options:

$$T_i(p_s, p_g) = T_i^{\text{Nav}}(p_s, p_g, M_i), \text{ if } R_i(p_s, p_g) < r_s, \quad (26)$$

which prevents unreachable assignments while enabling capability-aware request realization and task allocation; (II) *Failure detection and recovery.* As illustrated in Fig. 9, Failures are detected locally via bounded waiting times T_{\max}^- and T_{\max}^+ for predecessor- and successor-side checks, respectively; upon detection, the failed robot is removed and the wheel topology is restored through a small number of subsequent meetings, with $T_{\max}^+ > T_{\max}^-$ ensuring conservative successor-side detection. (III) *Spontaneous meeting events.* Unexpected encounters are accommodated by fusing local data while preserving the current topology; only inter-team meetings between neighboring teams trigger an update of the external-event schedule, whereas non-neighboring teams exchange data without additional coordination.

3) *Limitations:* Several limitations motivate future extensions. First, accurate map merging is essential for intermittent coordination, yet high merge reliability may require increased overlap when initial poses are uncertain, which conflicts with the objective of minimizing redundant exploration; this trade-off is not explicitly modeled. Then, the current system largely ignores semantic cues, which could improve region prioritization, automate request generation, and enhance map merging through semantic anchors, and is critical for missions such as search and rescue. For similar reasons, interaction is currently limited to touch or typing, which can be burdensome for non-expert users; multimodal interfaces, LLM-based command translation, and reusable request templates may improve usability and task coverage. Lastly, exploration efficiency remains sensitive to map topology; predictive mapping and learned heuristics could further improve frontier selection and communication-event placement [12], [13], accelerating both exploration and contingent task fulfillment.

TABLE III
EVALUATION OF KEY PARAMETERS UNDER DIFFERENT TEAM CONFIGURATION.

Metrics	op-1+4ro	op-2+4ro	op-1+2ro & op-2+2ro		
			$T_c = 240$	$T_c = 300$	$T_c = 360$
T_{op1} [s] ¹	585	-	553	413	466
T_{op2} [s] ¹	-	494	545	494	452
L_{op1} [m] ²	50.0	-	52.8	52.7	50.7
L_{op2} [m] ²	-	79.7	41.1	41.6	40.6
δ_{in} [s] ³	118	117	93	85	104
δ_{ext} [s] ⁴	-	-	276	335	371
M_c [%] ⁵	-	-	71.9	40.7	44.5

¹ Time when operator 1 or 2 receives the complete map.

² Distance travelled by the operator 1 or 2.

³ Maximum intra-team latency. ⁴ Maximum inter-team latency.

⁵ Percentage of overlapping area explored by both teams.

V. NUMERICAL EXPERIMENTS

For validation, extensive numerical simulations and hardware experiments are presented in this section. All components are implemented in Python and ROS and tested on a laptop with an Intel Core i7-1280P CPU. Simulation and experiment videos can be found in the supplementary files.

A. System Description

1) *System Setup:* Each robot $i \in \mathcal{N}$ builds a local SLAM map M_i using a 2D occupancy grid representation [49]. All simulations are conducted in ROS-Stage with gmapping, where robots use differential-drive navigation with the default ROS stack, with a maximum linear/angular speed of 1.0 m/s and 1.0 rad/s, and a sensing range of 15 m. Communication is intermittent and only enabled when the measured link quality exceeds 50 dB; the ground-truth quality follows an analytical propagation model [33] that is unknown to the planner, while a learned estimator predicts it from sampled measurements. Local maps are merged upon connectivity using `multirobot_map_merge` [14]. Operators interact with the fleet through a customized Rviz GUI as in Figure 8 to issue online requests and update the latency thresholds T_h^k and T_c at return events.

2) *Spatial-temporal Tree of Data Flow:* For concise visualization, we use a spatial-temporal tree of data flow (**SDF-tree**) in the x - y - t space, as shown in Fig. 10. Each explored grid cell is represented by a leaf node attached to the corresponding robot trajectory through an *E-edge*; once that information reaches the operator, the same node is linked to the operator trajectory by an *R-edge*, whose time-axis projection gives the latency. Communication events are shown by *M-edges*, while an *L-edge* marks the maximum latency within or between teams. In this way, the SDF-tree jointly records where a region is explored, when it is explored, and when it becomes available to the operator, so both exploration progress and information propagation can be read from the same structure.

B. Operator-in-the-loop Collaborative Exploration

To begin with, the requests ξ_1 , ξ_3 , and ξ_7 are investigated within two different scenarios for a single team and two teams, to validate the human-robot collaborative exploration framework under latency constraints.

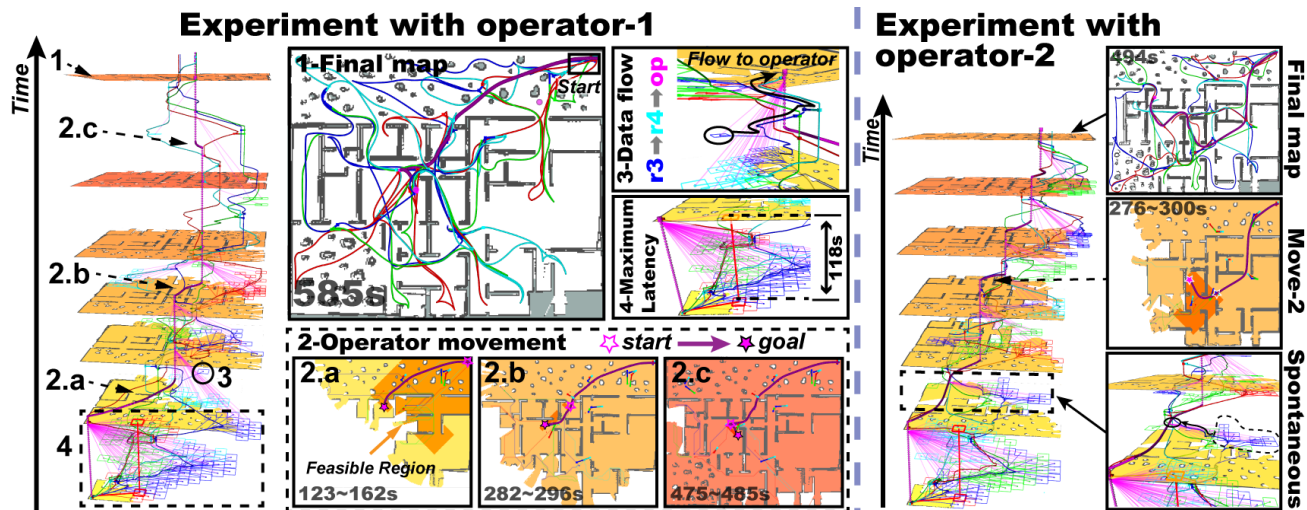


Fig. 11. Comparisons of the same team within Scenario-1 under two different behaviors of operators (Left and Right), visualized by the SDF-tree in addition to the local map of the operator at several return events. Notice the differences in the operator movement (thick lines) and the associated feasible region.

1) *Simulated Scenarios*: The following two scenarios of varying complexity and features are considered:

Scenario-1: as shown in Figure 11, the task is to explore a large building complex surrounded by forest area, which has a size of $60m \times 50m$. The operator is allowed to move only within the feasible region, and does not send any other request. The intra-team latency bound T_h^k is set to $120s$ for each team, and inter-team latency T_c is set to $300s$ for each pair of neighboring teams. A single team of four robots and one operator is tested first, and then extended to two teams with two robots per team.

Scenario-2: as shown in Figure 12, a $120m \times 90m$ large-scale subterranean environment, similar to the DARPA SubT setting in [35], is considered. It features lobby rooms connected by long, narrow passages with frequent sharp turns, and multiple branching structures with dead ends, which significantly degrades connectivity and poses challenges for communication-constrained exploration. Therefore, numerical validations are conducted under different team configurations, communication strategies, and operator motions. Specifically, two teams with 4 robots and 1 operator are tested and compared against a single team with 8 robots and 1 operator under different operator commands.

2) *Single-team in Scenario-1 under Distinct Operator Motion Patterns*: To validate the intra-team latency constraint, the proposed coordination scheme is evaluated for a single team in Scenario-1 with two operators exhibiting distinct motion behaviors (Fig. 11). In both cases, the maximum latency remains below the bound $T_h^k = 120s$, as each R-edge is consistently shorter than its corresponding L-edge, and full map coverage is achieved within a few hundred seconds. For the first operator, the grid cell inducing the largest latency is initially explored by robot 0 and delivered at the first return event after $118s$; the operator then moves toward the environment center via three consecutive motions at $123s$, $282s$, and $475s$, all within the feasible region. The exploration completes at $585s$, with 23 inter-robot meeting events and 7 return events. For the second operator, moving downward first and then toward the top-left region yields a shorter completion time of $494s$ while keeping the maximum latency at $115s$. This

speedup mainly results from mitigating late-stage long-range transmissions from corner regions and reducing the frequency of planned return events, as the operator remains closer to planned robot meeting points, leading to more spontaneous returns. Consequently, robots spend more time exploring rather than relaying data, despite a longer operator travel distance of $79.7m$ compared with $50.0m$ in the first case.

3) *Two Teams in Scenario-1 under Different T_c* : In Scenario-1, the inter-team coordination is evaluated with two teams initially deployed in close proximity and set $T_c = 300s$, where the first external exchange is triggered after operator separation and subsequent requests follow (20), and the results are shown in Fig. 12. As the two operators move in different directions, the teams explore largely complementary regions, and the first external communication allows messengers (robot 1 and robot 3) to merge their local maps at $382s$, substantially reducing redundant exploration. Consequently, operator-1 and operator-2 obtain the complete map at $413s$ and $494s$, respectively, with more than 60% of the area explored by only one team; moreover, operator-2's travel distance drops to around $40m$ compared with $80m$ in the single-team case. Throughout the run, latency guarantees are preserved, with maximum intra-team latencies of $76s$ and $85s$ and maximum inter-team latency of $284s$ (below $T_c = 300s$), indicating reliable inter-team information delivery under the combined inter-/intra-team bounds. As shown in Table III, further experiments varying T_c reveal a consistent efficiency gain over the single-team baseline but also a clear trade-off: overly small T_c induces premature exchanges that fuse maps before each team finishes exploiting nearby frontiers, increasing spatial overlap and coordination overhead, whereas overly large T_c delays information fusion and allows redundancy to re-emerge. Therefore, T_c plays a key role in balancing early synchronization cost against late sharing inefficiency.

4) *Two Teams in Scenario-2 with Different Operator Requests*: Scenario-2 evaluates inter-team latency constraints in a large subterranean environment with two teams, each consisting of one operator and four robots, and $T_c = 300s$ in Figs. 13 and 14. With migration and inter-team coordination enabled, both operators obtain the complete map at $1872s$

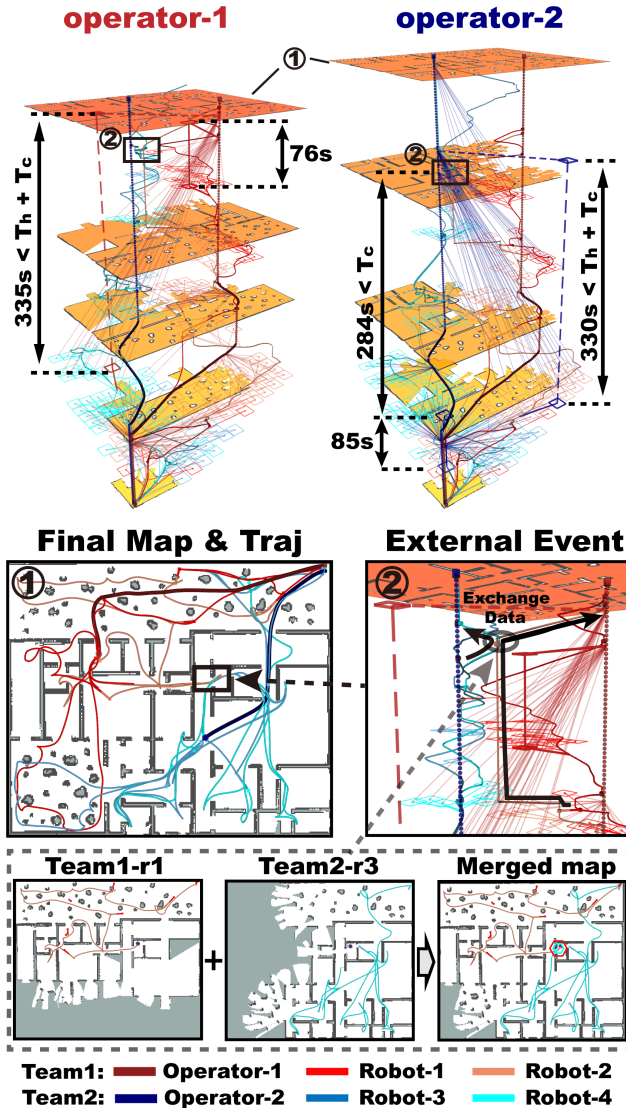


Fig. 12. Simulation results of two teams deployed in Scenario-1, where the latency constraints $T_c = 300s$. **Top:** the SDF-Trees of Team-1 and Team-2. Both contain all the robot trajectories, M-edges and E-edges, while the R-edges, L-edges and maps are linked to the corresponding operator. The L-edges with (without) dashed line represent maximum inter (intra)-team latency; **Middle:** the final map with trajectories of all robots and operators (Team-1 in red and Team-2 in blue) and one snapshot of an external communication event; **Bottom:** the local maps of Robot-1 in Team-1 and Robot-3 in Team-2 are merged during the external event.

while achieving complementary branch coverage: team-1 and team-2 explore 59.2% and 67.4% of the environment with only 26.6% overlap, and operators travel 139.4m and 145.0m, respectively. These results highlight two factors for scalability in this branched topology. First, migration is necessary when feasible-region motion alone cannot reach new frontiers; without it, exploration stalls early and the final exploration rate drops to 32.6% for one team of eight robots and 58.5% for two teams of four robots. Second, explicit inter-team coordination under latency constraints is critical for efficiency rather than mere completion: removing it still allows completion under migration, but overlap rises from 26.6% to 84.0% and completion slows from 1872s to 2433s. Moreover, although migration enables reliable completion across configurations, a single team of eight robots remains slower and finishes

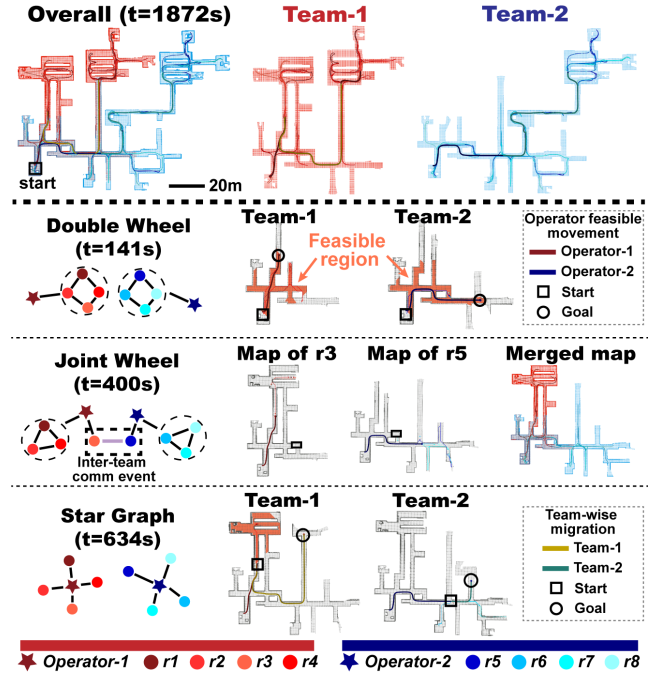


Fig. 13. Simulation results of two teams deployed in a large subterranean environment for Scenario-2, where the latency $T_h = 120s$ and $T_c = 300s$. **Top:** the explored area of each team within the final map for Team-1 (red) and Team-2 (blue), including the trajectories for robots and operators; **Bottom:** the evolution of embedded graphs for both teams over time.

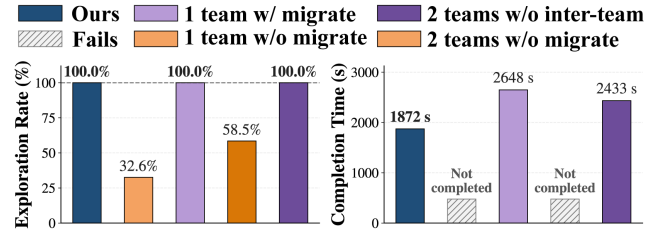


Fig. 14. Comparison of exploration rate (Left) and completion time (Right) for the fleet of single and two teams with and without “migrate” requests.

at 2648s, underscoring the benefit of multi-team parallelism for covering multiple branches simultaneously.

C. Multi-Modal Requests and Topology Adaptation

In this part, the proposed framework is evaluated regarding various multi-modal online requests that require the fleet to transit among different communication topologies.

1) *Simulated Scenario:* Two teams are deployed to explore an office environment of size $90m \times 70m$, where each team is composed of 4 robots and one operator. In addition to exploration, in total 5 tasks are scattered in the environment, the completion of which require the proposed CEC chain. As summarized in Table IV, these tasks include the inspection of a target area, the direct assistance to a robot, and to control a robot remotely to open a door. During the experiment, each operator can specify any type of requests, including ξ_2, ξ_3, ξ_4 and the migration command; when a robot observes a task, it can send requests of type ξ_5 or ξ_6 to the operator in order to fulfill the task. Initially, both teams are located at the top end of a corridor, and the exploration starts after the first round of communication. The latency constraints T_h and T_c are set to 120s and 600s, respectively.

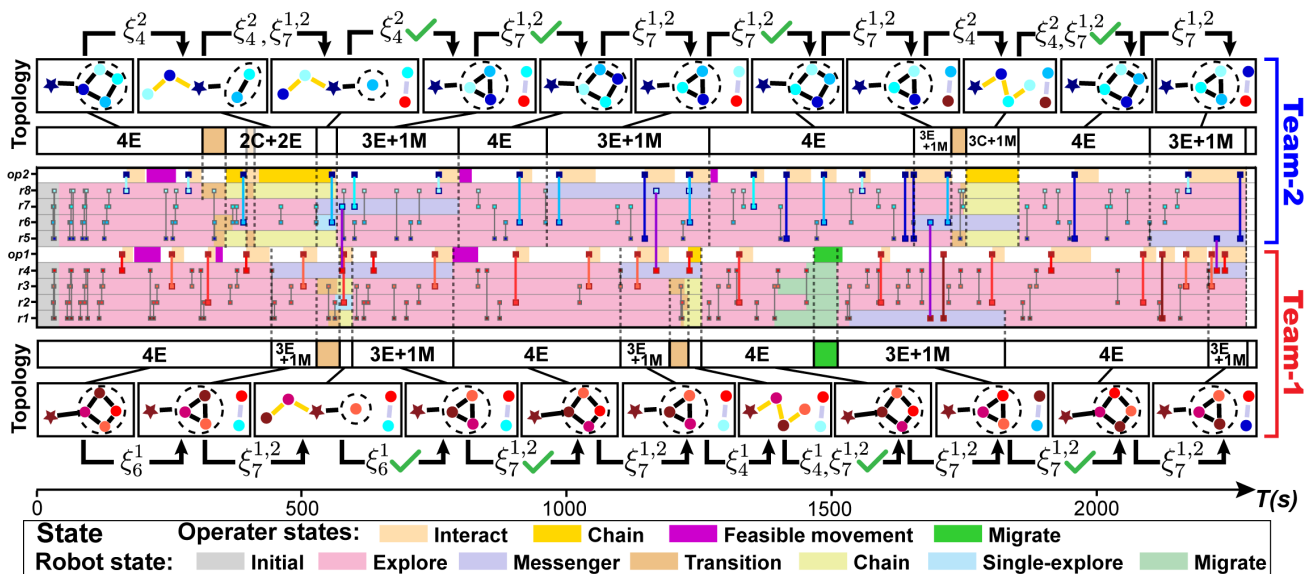


Fig. 15. Simulation results of two teams (2 operators and 8 robots) fulfilling 5 contingent requests via graph transitions, while exploring a $90m \times 70m$ office environment. **Top** and **Bottom**: the complete evolution of the operation state and the associated communication graphs of Team-2 and Team-1 after each request is activated and fulfilled, respectively; **Middle**: the intermittent intra-team and inter-team communication events between the corresponding robots and operators (dumbbell-shaped vertical lines). The communication graph is specified by the number of robots and their operation mode, where ‘E’, ‘C’ and ‘M’ represent the exploration, chain, and messenger state respectively, i.e., “2E+2C” means 2 robots in the exploration state and 2 robots in the chain state.

TABLE IV
SUMMARY OF THE CONTINGENT TASKS, ALONG WITH THE ASSOCIATED ONLINE REQUESTS.

Task	Type	Request	Robots	$T_{tra}[s]^1$	$T_{sta}[s]^2$	$T_{dur}[s]^3$
Task-1	Inspection	ξ_4^2	r5, r8	44	356	39
Task-2	Inspection	ξ_4^2	r5, r8	16	411	152
Task-3	Assistance	ξ_6^1	r1, r3	43	572	24
Task-4	Push door	ξ_4^1	r1, r2, r3	35	1231	25
Task-5	Inspection	ξ_4^2	r5, r7, r8	28	1755	99

¹ Transition time from the joint wheel to chain graph.

² Starting time of the task execution. ³ Duration of the task.

2) *Results*: Figure 1, 15 and Table IV show that the framework can execute heterogeneous online requests with frequent graph reconfiguration while keeping the overall process efficient. All five tasks are successfully fulfilled by 1854s, including four operator-issued requests via ξ_4 and one robot-issued request ξ_6^1 , indicating that both human-initiated and robot-initiated tasking are handled without compromising completion. Crucially, the computational overhead of topology selection is negligible relative to physical execution: constructing the task-specific target graph set (CEC chain) takes 0.3s on average and matching process takes 0.1s, whereas the task execution itself spans 25s–152s, with inspection tasks requiring 39s–152s and assistance or door-opening taking around 25s. This separation in timescales confirms that performance is bottlenecked by task actions rather than planning or graph matching. Despite 11 graph transitions per team, reconfiguration remains tractable, with wheel-to-chain transitions completed within 34s–42s for chain lengths 3 and 2, respectively, and with the most efficient case achieving a direct task-to-task transition of only 16s. Compared with the average wheel–chain transition time of 38s, this highlights that the framework can exploit topological similarity across consecutive tasks to reduce reconfiguration latency. More-

over, the system maintains bounded inter-team information exchange under repeated reconfiguration, evidenced by only four external communication events at 574s, 1167s, 1683s, and 2224s, while both operators still obtain complete maps at 2242s and 2290s. These results substantiate that topology adaptation scales to frequent online tasking, with planning costs at the sub-second level and transition costs that remain small compared with task durations.

D. Comparisons

The proposed framework, denoted as **MOROCCO**, is compared against representative baselines in both single-team and multi-team settings. Since existing methods cannot jointly support collaborative exploration and consistent tasks, the comparison focuses on collaborative exploration under bounded-latency operator updates.

1) *Single-team Experiments*: A single team consisting of one operator and four robots is evaluated first in three environments under the same request ξ_1^k with $T_h = 160s$, repeating each method over five runs. As most baselines do not explicitly enforce operator-update latency, they are minimally adapted to satisfy T_h by inserting return events while preserving their original exploration policies. Baselines include **CMRE** [10], **M-TARE** [50], **JSSP** [39], and **MOROCCO-NI** that disables online human-robot interaction. Details of the baselines and the adaptation are described in the Supplementary file.

Table V and Fig. 16 reveal a consistent trend across all environments. CMRE and M-TARE typically expand rapidly at early stages but become effectively range-limited once periodic returns are imposed, causing map updates to stagnate after roughly 400s and resulting in incomplete coverage, e.g., around 50% in the building environment. JSSP further degrades under the same constraint due to suboptimal rendezvous and waiting behaviors, yielding even lower coverage. MOROCCO-NI substantially improves coverage and reduces

TABLE V

SINGLE-TEAM RESULTS IN THREE SCENARIOS (AVERAGED OVER 5 RUNS).

Environment	Method	CA ¹	ER ²	Eff ³	LU ⁴	RR ⁵	Int ⁶
Building 60m × 50m	CMRE	1433	50.5	2.4	432.8	3.8	no
	M-TARE	1442	50.8	2.4	445.5	3.7	no
	JSSP	1323	46.6	2.2	425.5	2.9	no
	MOROCCO-NI	2146	75.6	3.6	449.6	2.1	no
	MOROCCO	2838	100	4.7	573.5	1.4	yes
Cave 65m × 57m	CMRE	1233	63.1	1.1	433.6	3.8	no
	M-TARE	1397	71.5	1.3	556.0	4.0	no
	JSSP	813	28.0	0.7	500.8	2.5	no
	MOROCCO-NI	1572	80.5	1.4	875.2	1.75	no
	MOROCCO	1953	100	1.8	1027.1	1.1	yes
Indoor 120m × 90m	CMRE	562	19.3	0.2	543.2	3.6	no
	M-TARE	564	19.4	0.2	484.5	3.5	no
	JSSP	580	19.9	0.2	495.6	2.9	no
	MOROCCO-NI	966	33.2	0.3	473.1	2.1	no
	MOROCCO	2908	100	1.0	2818.0	1.4	yes

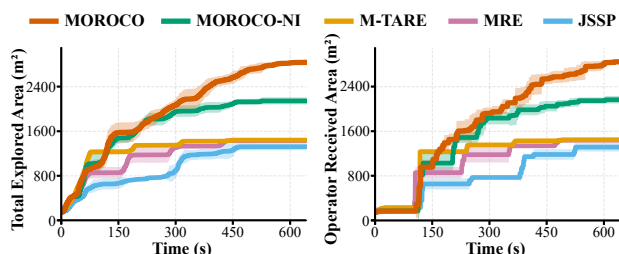
¹ CA: explored area in m². ² ER: exploration rate in %.³ Eff: exploration efficiency in m²/s.⁴ LU: last update time in s. ⁵ RR: return rate in #/T_h.⁶ Int: whether operator-robot interaction is supported.

Fig. 16. Evolution of the explored area (Left) and the operator-received area (Right), via the proposed method and baseline methods in the building complex scenarios, averaged over 5 runs.

the return rate, indicating more efficient information propagation under the latency constraint; however, it still fails to reliably complete large environments without online operator guidance. In contrast, MOROCO achieves 100% coverage in all three environments while maintaining the *lowest return rate* and timely operator updates, showing that bounded-latency exploration requires not only compliant return scheduling but also tight coupling between exploration and communication together with online human-in-the-loop intervention.

2) *Multi-team Experiments*: Because no existing baseline simultaneously addresses intra-team and inter-team latency constraints, MOROCO is compared against three controlled ablations: **MO-NM** without migrate, **MO-NP** without prioritized-regions, and **MO-NE** without external events and inter-team latency enforcement. Besides, a naive extension of the single-team baseline CMRE to multi-teams is also tested for comparison, denoted as **M-CMRE**. All methods are evaluated using two teams with two robots and one operator per team under $T_h = 160s$ and $T_c = 360s$, over five runs.

As summarized in Table VI, MOROCO consistently delivers the strongest overall performance, combining full coverage with shorter mission times, reduced inter-team overlap, and inter-team latency strictly within T_c . The naive M-CMRE presents the lowest coverage due to static operator, and highest overlap as it lacks any mechanism for inter-team coordination. The ablations isolate the functional necessity of each component. Without migrate, MO-NM may terminate prematurely

TABLE VI

TWO-TEAM RESULTS IN THREE SCENARIOS (AVERAGED OVER 5 RUNS).

Environment	Method	EA(m ²) ¹	MT(s) ²	ET(s) ³	IL(s) ⁴	PO(%) ⁵
Building 60m × 50m	M-CMRE	1453.2	–	–	0.0	82.4
	MO-NM	2837.0	493.5	420.0	321.4	48.5
	MO-NP	2819.7	588.7	570.7	202.1	76.6
	MO-NE	2833.6	582.7	546.4	359.0	63.2
	MOROCCO	2838.1	478.3	413.5	280.8	47.0
Cave 65m × 57m	M-CMRE	1426.1	–	–	0.0	83.1
	MO-NM	1930.3	1023.0	952.8	287.2	63.0
	MO-NP	1955.7	1047.2	995.6	250.6	79.2
	MO-NE	1936.7	952.7	856.0	482.7	71.4
	MOROCCO	1958.4	806.1	724.4	305.4	57.3
Indoor 120m × 90m	M-CMRE	572.5	–	–	0.0	73.0
	MO-NM	1873.7	–	–	328.9	64.7
	MO-NP	2748.6	2036.1	1830.8	346.7	70.7
	MO-NE	2712.0	2008.9	2005.5	1030.3	72.6
	MOROCCO	2779.0	1935.3	1865.2	319.4	56.2

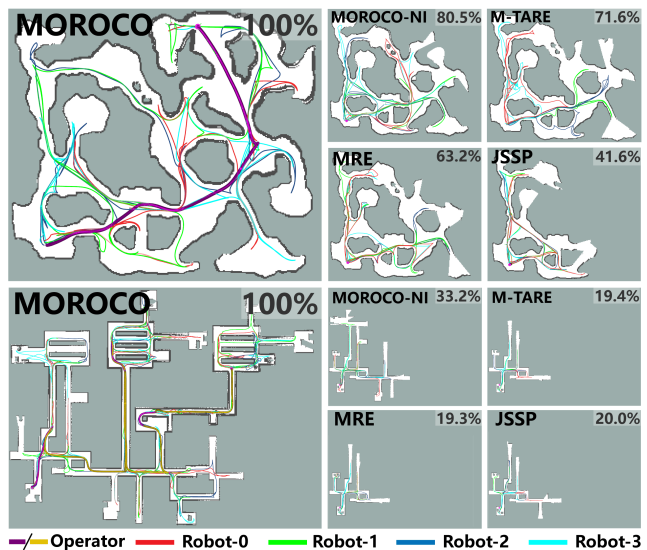
¹ Total explored area. ² Mission time. ³ Exploration termination time.⁴ Maximum inter-team latency. ⁵ Percentage of overlapping area.

Fig. 17. Final maps obtained by the operator (Left), and the trajectories of the operator and all robots (Right) in the cave (Top) and indoor scenarios (Bottom), under the proposed method and four baselines.

in constrained topologies such as the indoor environment, preventing completion. Without prioritized regions, MO-NP induces substantial redundancy, with overlap exceeding 70% in smaller environments where the teams would otherwise interfere. Without enforced external exchanges, MO-NE exhibits rapidly increasing inter-team latency as the environment scales, exceeding $T_c = 360s$ and degrading operator update timeliness and exploration efficiency. Collectively, these results indicate that migrate, operator-directed spatial decoupling, and latency-constrained inter-team coordination are jointly required to sustain efficient multi-team exploration under bounded-latency updates.

E. Generalizations

This experiment validates key generalizations of the proposed framework in a single setting, including adaptation to heterogeneous fleets, online recovery from robot failures, and scalability to multiple teams.

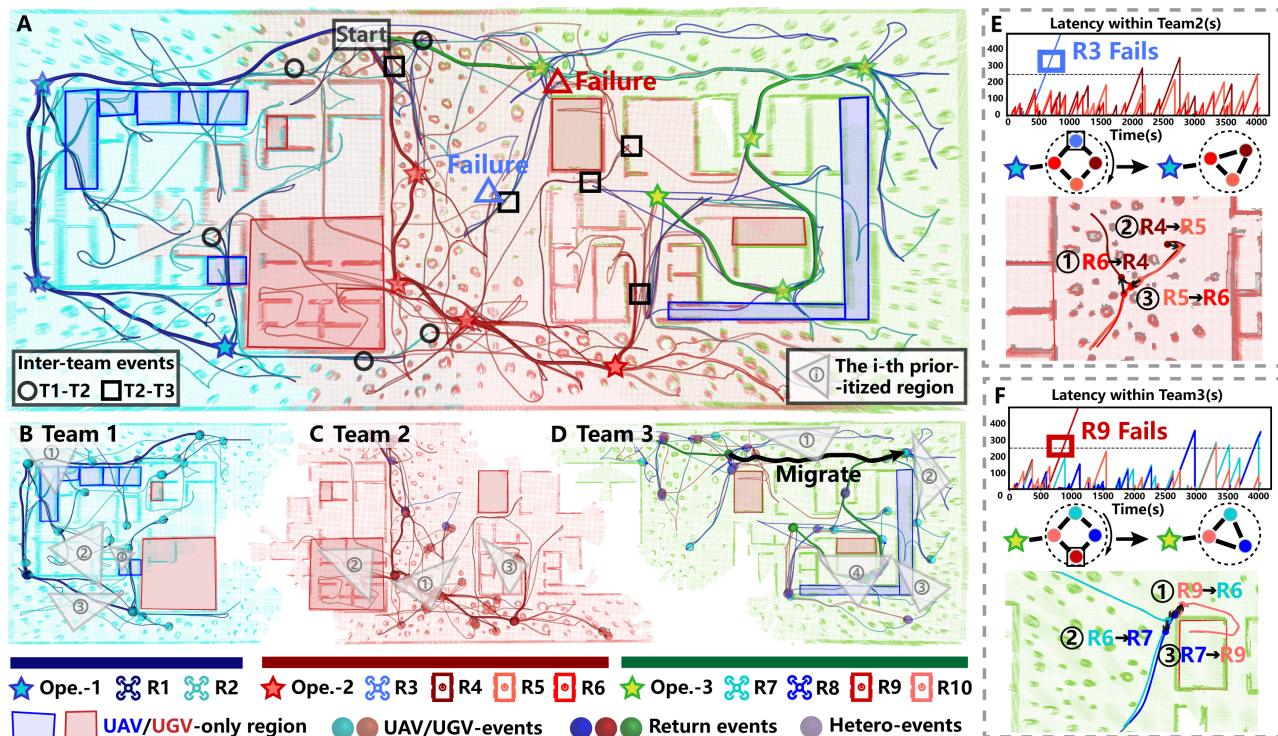


Fig. 18. Simulation results of **three teams** composed of heterogeneous robots collaboratively exploring a large and complex environment and meanwhile dealing with *potential robot failures*. (A): the complete final map colored with contributions from each team, the trajectories of operators (thicker lines) and robots (thinner lines), the positions of external events between neighboring teams, and the regions reachable by only one type of robots; (B)-(D): the trajectories of each team and positions of communication events colored by its type, as well as the prioritized regions ordered by time. (E)-(F): the failure detection and recovery process for Team-2 and Team-3.

1) *Simulated Scenario*: As shown in Fig. 18, three teams with 10 robots and 3 operators collaboratively explore a large environment containing both UAV-only and UGV-only accessible regions. UAVs and UGVs have different mobility limits, with maximum speeds of 1.2 m/s and 0.8 m/s , respectively. Inter-team communication follows a sparse line graph in which team-1 and team-3 communicate through team-2. The latency bounds are set to $T_h = 250\text{ s}$ and $T_c = 500\text{ s}$, and unexpected robot failures may occur during execution, with waiting-time bounds $T_{\max}^+ = 60\text{ s}$ and $T_{\max}^- = 30\text{ s}$.

2) *Results*: The results in Fig. 18 confirm that the framework generalizes to heterogeneous multi-team exploration while preserving bounded-latency information propagation under failures. First, heterogeneous constraints are respected at execution time: planned and realized coordination events occur only at locations simultaneously reachable by the involved robot types, and the final exploration pattern demonstrates capability-aware allocation, where UAV-heavy teams naturally expand into UAV-only regions while UGV resources focus on height-constrained areas, reducing unnecessary detours in mixed-access structures. Second, the system remains resilient to robot dropouts and continues exploration with limited disruption. Robot-2 in team-2 fails at 356 s and is detected after the 30 s waiting bound, after which coordination proceeds with an updated 3-robot intra-team topology; robot-8 in team-3 fails at 606 s , is detected after the 60 s waiting bound, and is fully recovered after 3 subsequent meeting events through message propagation and topology update. Despite these failures, exploration still completes at around 3600 s and the workload remains balanced across teams, with explored-

area ratios of 45%, 51%, and 56%. Most importantly, latency guarantees are preserved throughout, with maximum inter-team latencies of 485 s and 472 s below $T_c = 500\text{ s}$, and maximum intra-team latencies of 244 s , 221 s , and 237 s below $T_h = 250\text{ s}$ for all non-failed robots and non-messenger robots. It can be seen that the proposed scheme scales to multiple teams with heterogeneous capabilities and maintains bounded-latency coordination even under online topology reconfiguration induced by failures.

F. Hardware Experiments

To further validate the proposed method in real-world conditions, hardware experiments are conducted with a heterogeneous fleet and multiple operators. More experimental details can be found in the supplementary video.

1) *System setup*: The experiments are performed in a standard office environment of size $100\text{ m} \times 30\text{ m}$ with rooms and corridors, with no pre-installed communication infrastructure. The fleet consists of three Scout-mini ground robots and one Cobot-kit mobile manipulator, deployed as two teams, each with two robots and one operator. Each Scout-mini is equipped with a 16-line lidar, an IMU, and an onboard Nvidia Xavier computer, running fast-lio2 [51] at 10 Hz to build a 3D point-cloud map that is converted to a 2D occupancy grid map via octomap [52] for planning. The mobile manipulator runs hdl_graph_slam [53] for lidar-based SLAM, and all robots carry an Intel RealSense D435 camera for inspection and tele-operation. Robot navigation uses move_base with a maximum speed of 0.5 m/s , and communication relies on range-limited FT-Dlink ad-hoc devices. Each operator carries

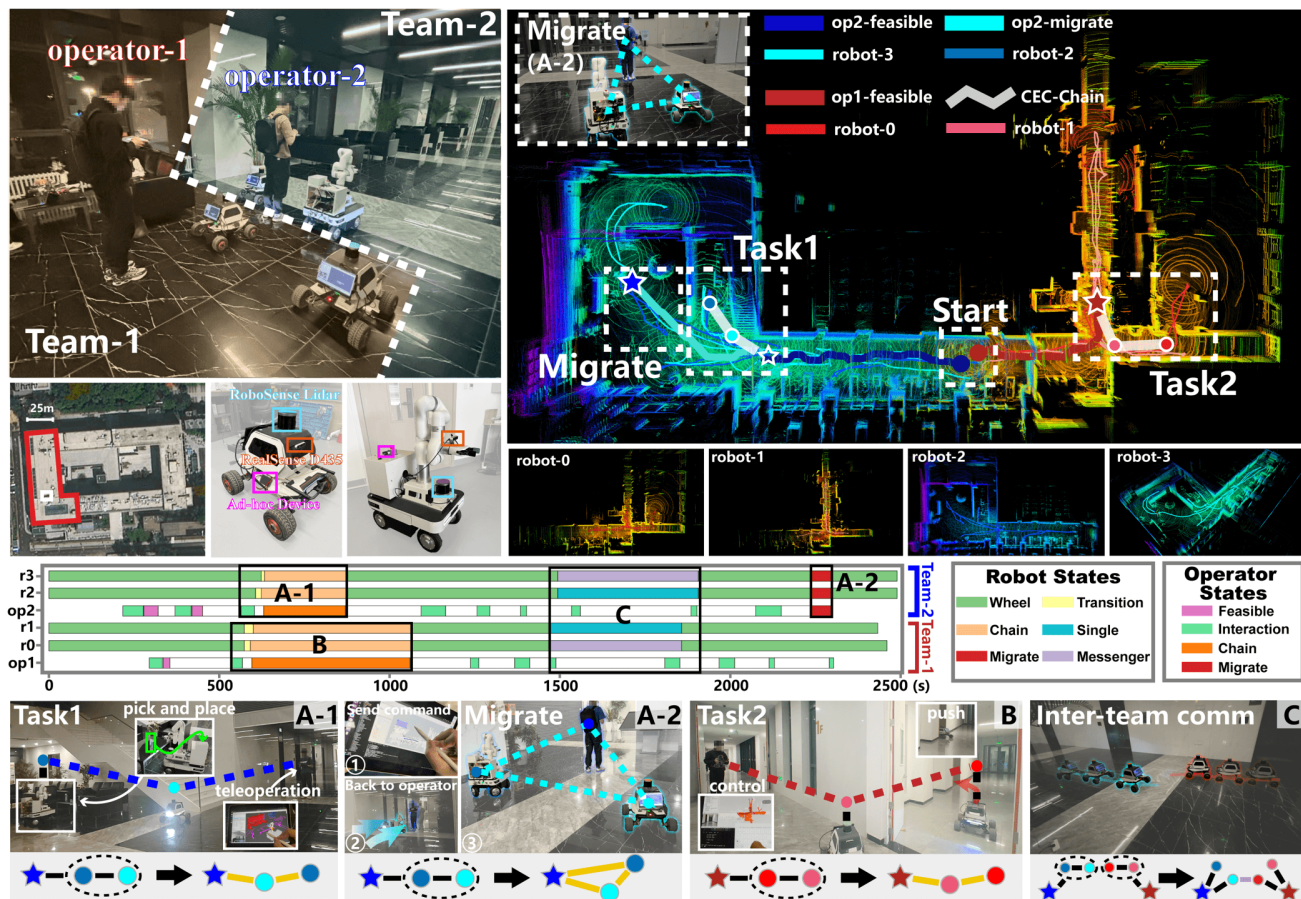


Fig. 19. **Top-left:** the experimental environment and the heterogeneous robot teams. Team-1 consists of 2 ground robots, while team-2 consists of 1 ground robot and 1 mobile manipulator. Local communication is enabled via the FT-DLink ad-hoc device. **Top-right:** the final merged map at the end of the mission, and the local maps explored by each robot. Trajectories of the operators are indicated by the thick lines, starting from the initial location and ending at the solid stars, while the thin lines represent the trajectories of the robots. **Middle:** The evolution of communication graphs in both teams during the whole mission. **Bottom:** Snapshots of key moments and graph transitions during the mission.

a laptop for computation and a lightweight Android tablet for visualization and issuing online requests through the GUI. Teams are initialized at the same corner of the environment with a shared coordinate system; the intra-team latency is set to $T_h = 300s$ and the inter-team latency is set to $T_c = 1800s$.

2) *Results:* As shown in Fig 19, two teams successfully explore the office environment and the operators obtain a complete map after about 2500s, covering $1072m^2$. Timely operator situational awareness is maintained through return events, with 9 returns per team and maximum update latencies of 287s and 263s respectively, both below the prescribed bound $T_h = 300s$. Inter-team coordination further improves efficiency: the inter-team communication event occurs at 1565s, satisfying $T_c = 1800s$, and limits redundant exploration to $92m^2$, corresponding to 8.6% overlap. Beyond exploration, two operator-handled tasks further demonstrate the effectiveness of the proposed interaction mechanism under constrained connectivity. First, the “push door and inspect” task is executed by Operator-1 in Team-1. After Operator-1 issues the request ξ_4^1 , the graph matching process takes 3.1s to generate a feasible plan, and it takes 27s for the two robots to reach the assigned locations. Then, a smooth video stream from Robot-0 is transmitted to Operator-1 to support teleoperation for door pushing and inspection. Second, the “pick and place” task is executed by Operator-2 in Team-2, who

teleoperates the Cobot-kit mobile manipulator (Robot-2) to pick and place a bottle on the table. The graph matching takes 2.8s and transition takes 26s, which ensures that the mobile manipulator is assigned as the end robot in the chain. Then, robots 2 and 3 form a connected line graph, enabling Operator-2 to perform the task using a customized tablet GUI that provides (i) a video stream from the gripper-mounted camera, (ii) the local point cloud around the manipulator, and (iii) a MoveIt interface for remote tele-operation. With this support, Operator-2 completes this task in 240s. Lastly, Team-2 performs a team-wise migration as a star graph at 2243s for further exploration. Overall, the latency-bounded updates via the intermittent communication have shown to be essential for the operators to make informed decisions, while the graph decomposition enables online request fulfillment.

VI. CONCLUSION

This work presented MoRoCo, an online topology-adaptive framework for multi-operator multi-robot coordination under restricted communication. Built on a latency-bounded intermittent communication backbone, MoRoCo enables collaborative exploration and online request servicing through dynamic graph reconfiguration using only local communication. Simulations and hardware experiments demonstrated its effectiveness in communication-restricted environments.

Future work will address robustness to uncertain map merging, richer semantic and multimodal interaction, and topology-aware exploration strategies under restricted communication.

REFERENCES

- [1] M. S. Couceiro, "An overview of swarm robotics for search and rescue applications," *Artif. Intell.: Concepts, Methodol., Tools, Appl.*, pp. 1522–1561, 2017.
- [2] F. Klaesson, P. Nilsson, T. S. Vaquero, S. Tepsuporn, A. D. Ames, and R. M. Murray, "Planning and optimization for multi-robot planetary cave exploration under intermittent connectivity constraints," in *Proc. ICAPS Workshop Planning Robot.*, 2020.
- [3] A. Hussein, M. Adel, M. Bakr, O. M. Shehata, and A. Khamis, "Multi-robot task allocation for search and rescue missions," in *J. Phys.: Conf. Ser.*, vol. 570, no. 5, 2014, p. 052006.
- [4] R. G. Colares and L. Chaimowicz, "The next frontier: Combining information gain and distance cost for decentralized multi-robot exploration," in *Proc. ACM Symp. Appl. Comput.*, 2016, pp. 268–274.
- [5] B. Zhou, H. Xu, and S. Shen, "Racer: Rapid collaborative exploration with a decentralized multi-uav system," *IEEE Trans. Robot.*, vol. 39, no. 3, pp. 1816–1835, 2023.
- [6] E. Tolstaya, J. Paulos, V. Kumar, and A. Ribeiro, "Multi-robot coverage and exploration using spatial graph neural networks," in *Proc. IEEE/RSJ Int. Conf. Intell. Robots Syst.*, 2021, pp. 8944–8950.
- [7] B. Yamauchi, "A frontier-based approach for autonomous exploration," in *Proc. IEEE Int. Symp. Comput. Intell. Robot. Autom.*, 1997, pp. 146–151.
- [8] B. Yamauchi, "Decentralized coordination for multirobot exploration," *Robot. Auton. Syst.*, vol. 29, no. 2, pp. 111–118, 1999.
- [9] Q. Bi, X. Zhang, J. Wen, Z. Pan, S. Zhang, R. Wang, and J. Yuan, "Cure: A hierarchical framework for multi-robot autonomous exploration inspired by centroids of unknown regions," *IEEE Trans. Autom. Sci. Eng.*, vol. 21, no. 3, pp. 3773–3786, 2024.
- [10] W. Burgard, M. Moors, C. Stachniss, and F. E. Schneider, "Coordinated multi-robot exploration," *IEEE Trans. Robot.*, vol. 21, no. 3, pp. 376–386, 2005.
- [11] S. Baek, B. Moon, S. Kim, M. Cao, C. Ho, S. Scherer, and J. H. Jeon, "Pipe planner: Pathwise information gain with map predictions for indoor robot exploration," in *Proc. IEEE/RSJ Int. Conf. Intell. Robots Syst.*, 2025, pp. 7684–7691.
- [12] G. Calzolari, V. Sumathy, C. Kanellakis, and G. Nikolakopoulos, "Reinforcement learning driven multi-robot exploration via explicit communication and density-based frontier search," in *Proc. IEEE Int. Conf. Robot. Autom.*, 2025, pp. 11 406–11 412.
- [13] A. Sygkounas, D. Tspianitis, G. Nikolakopoulos, and C. P. Bechlioulis, "Multi-agent exploration with reinforcement learning," in *Proc. IEEE Mediterranean Conf. Control Autom. (MED)*, 2022, pp. 630–635.
- [14] J. Hörner, "Map-merging for multi-robot system," Prague, 2016.
- [15] S. Yu, C. Fu, A. K. Gostar, and M. Hu, "A review on map-merging methods for typical map types in multiple-ground-robot slam solutions," *Sensors*, vol. 20, p. 6988, 12 2020.
- [16] A. Asgharivaskasi, F. Girke, and N. Atanasov, "Riemannian optimization for active mapping with robot teams," *IEEE Trans. Robot.*, vol. 41, pp. 1077–1097, 2025.
- [17] X. Liu, J. Lei, A. Prabhu, Y. Tao, I. Spasojevic, P. Chaudhari, N. Atanasov, and V. Kumar, "Slideslam: Sparse, lightweight, decentralized metric-semantic slam for multirobot navigation," *IEEE Trans. Robot.*, vol. 41, pp. 6529–6548, 2025.
- [18] J. M. Esposito and T. W. Dunbar, "Maintaining wireless connectivity constraints for swarms in the presence of obstacles," in *Proc. IEEE Int. Conf. Robot. Autom.*, 2006, pp. 946–951.
- [19] M. T. Ohradzansky, E. R. Rush, D. G. Riley, A. B. Mills, S. Ahmad, S. McGuire, H. Biggie, K. Harlow, M. J. Miles, E. W. Frew *et al.*, "Multi-agent autonomy: Advancements and challenges in subterranean exploration," *Field Robot.*, vol. 2, pp. 1068–1104, 2022.
- [20] N. Dahlquist, S. Nordström, N. Stathouloupoulos, B. Lindqvist, A. Saradagi, and G. Nikolakopoulos, "Deployment of an aerial multi-agent system for automated task execution in large-scale underground mining environments," *IEEE Trans. Field Robot.*, vol. 2, pp. 465–484, 2025.
- [21] M. Al Khawaldah and A. Nüchter, "Enhanced frontier-based exploration for indoor environment with multiple robots," *Adv. Robot.*, vol. 29, no. 10, pp. 657–669, 2015.
- [22] J. Yu, J. Tong, Y. Xu, Z. Xu, H. Dong, T. Yang, and Y. Wang, "Smmr-explore: Submap-based multi-robot exploration system with multi-robot multi-target potential field exploration method," in *Proc. IEEE Int. Conf. Robot. Autom.*, 2021, pp. 8779–8785.
- [23] Y. Pei, M. W. Mutka, and N. Xi, "Connectivity and bandwidth-aware real-time exploration in mobile robot networks," *Wireless Commun. Mob. Comput.*, vol. 13, no. 9, pp. 847–863, 2013.
- [24] C. Wang, C. Yu, X. Xu, Y. Gao, X. Yang, W. Tang, S. Yu, Y. Chen, F. Gao, Z. Jian, X. Chen, F. Gao, B. Zhou, and Y. Wang, "Multi-robot system for cooperative exploration in unknown environments: A survey," *arXiv preprint arXiv:2503.07278*, 2025.
- [25] A. H. Tan, S. Narasimhan, and G. Nejat, "4cnet: A diffusion approach to map prediction for decentralized multi-robot exploration," *IEEE Trans. Robot.*, pp. 1–17, 2026.
- [26] T. Vaquero, M. Troesch, and S. Chien, "An approach for autonomous multi-rover collaboration for mars cave exploration: Preliminary results," in *Proc. Int. Symp. Artif. Intell., Robot. Autom. Space*, 2018.
- [27] K. Cesare, R. Skeele, S.-H. Yoo, Y. Zhang, and G. Hollinger, "Multi-uav exploration with limited communication and battery," in *Proc. IEEE Int. Conf. Robot. Autom.*, 2015, pp. 2230–2235.
- [28] Y. Marchukov and L. Montano, "Fast and scalable multi-robot deployment planning under connectivity constraints," in *Proc. IEEE Int. Conf. Auton. Robot Syst. Compet.*, 2019, pp. 1–7.
- [29] Y. Gao, Y. Wang, X. Zhong, T. Yang, M. Wang, Z. Xu, Y. Wang, Y. Lin, C. Xu, and F. Gao, "Meeting-merging-mission: A multi-robot coordinate framework for large-scale communication-limited exploration," in *Proc. IEEE/RSJ Int. Conf. Intell. Robots Syst.*, 2022, pp. 13 700–13 707.
- [30] M. A. Schack, J. G. Rogers, and N. T. Dantam, "The sound of silence: Exploiting information from the lack of communication," *IEEE Robot. Autom. Lett.*, vol. 9, no. 7, pp. 6736–6743, 2024.
- [31] Y. Kantaros, M. Guo, and M. M. Zavlanos, "Temporal logic task planning and intermittent connectivity control of mobile robot networks," *IEEE Trans. Autom. Control*, vol. 64, no. 10, pp. 4105–4120, 2019.
- [32] M. M. Zavlanos, M. B. Egerstedt, and G. J. Pappas, "Graph-theoretic connectivity control of mobile robot networks," *Proc. IEEE*, vol. 99, no. 9, pp. 1525–1540, 2011.
- [33] R. J. Marcotte, X. Wang, D. Mehta, and E. Olson, "Optimizing multi-robot communication under bandwidth constraints," *Auton. Robots.*, vol. 44, no. 1, pp. 43–55, 2020.
- [34] L. Xia, B. Deng, J. Pan, X. Zhang, P. Duan, B. Zhou, and H. Cheng, "Relink: Real-time line-of-sight-based deployment framework of multi-robot for maintaining a communication network," *IEEE Robot. Autom. Lett.*, vol. 8, no. 12, pp. 8152–8159, 2023.
- [35] M. Saboia, L. Clark, V. Thangavelu, J. A. Edlund, K. Otsu, G. J. Correa, V. S. Varadharajan, A. Santamaria-Navarro, T. Touma, A. Bouman *et al.*, "Achorde: Communication-aware multi-robot coordination with intermittent connectivity," *IEEE Robot. Autom. Lett.*, vol. 7, no. 4, pp. 10 184–10 191, 2022.
- [36] D. G. Riley and E. W. Frew, "Fielded human-robot interaction for a heterogeneous team in the darpa subterranean challenge," *ACM Trans. Human-Robot Interact.*, vol. 12, pp. 1 – 24, 2023.
- [37] Z. Zhang, J. Yu, J. Tang, Y. Xu, and Y. Wang, "Mr-topomap: Multi-robot exploration based on topological map in communication restricted environment," *IEEE Robot. Autom. Lett.*, vol. 7, no. 4, pp. 10 794–10 801, 2022.
- [38] Z. Tian, Y. Zhang, J. Wei, and M. Guo, "iHERO: Interactive human-oriented exploration and supervision under scarce communication," in *Proc. Robot.: Sci. Syst.*, 2024.
- [39] A. R. Da Silva, L. Chaimowicz, T. C. Silva, and M. A. Hsieh, "Communication-constrained multi-robot exploration with intermittent rendezvous," in *Proc. IEEE/RSJ Int. Conf. Intell. Robots Syst.*, 2024, pp. 3490–3497.
- [40] M. Corah, C. O'Meadhra, K. Goel, and N. Michael, "Communication-efficient planning and mapping for multi-robot exploration in large environments," *IEEE Robot. Autom. Lett.*, vol. 4, no. 2, pp. 1715–1721, 2019.
- [41] R. Bai, S. Yuan, K. Li, H. Guo, W.-Y. Yau, and L. Xie, "Realm: Real-time line-of-sight maintenance in multi-robot navigation with unknown obstacles," in *Proc. IEEE Int. Conf. Robot. Autom.*, 2025, pp. 7363–7369.
- [42] A. Dahiya, A. M. Aroyo, K. Dautenhahn, and S. L. Smith, "A survey of multi-agent human-robot interaction systems," *Robot. Auton. Syst.*, vol. 161, p. 104335, 2023.
- [43] J. Chen, B. Sun, M. Pollefeys, and H. Blum, "A 3d mixed reality interface for human-robot teaming," in *Proc. IEEE Int. Conf. Robot. Autom.*, 2024, pp. 11 327–11 333.

- [44] V. Villani, B. Capelli, C. Secchi, C. Fantuzzi, and L. Sabattini, “Humans interacting with multi-robot systems: a natural affect-based approach,” *Auton. Robots.*, vol. 44, pp. 601–616, 2020.
- [45] S. Thrun, “Probabilistic robotics,” *Commun. ACM*, vol. 45, no. 3, pp. 52–57, 2002.
- [46] Y. Tian, Y. Chang, F. H. Arias, C. Nieto-Granda, J. P. How, and L. Carlone, “Kimera-multi: Robust, distributed, dense metric-semantic slam for multi-robot systems,” *IEEE Trans. Robot.*, vol. 38, no. 4, 2022.
- [47] R. Burkard, M. Dell’Amico, and S. Martello, *Assignment Problems*. Society for Industrial and Applied Mathematics, 2012.
- [48] G. OR-Tools, <https://github.com/google/or-tools>, 2022.
- [49] H. Moravec and A. Elfes, “High resolution maps from wide angle sonar,” in *Proc. IEEE Int. Conf. Robot. Autom.*, vol. 2, 1985, pp. 116–121.
- [50] C. Cao, H. Zhu, Z. Ren, H. Choset, and J. Zhang, “Representation granularity enables time-efficient autonomous exploration in large, complex worlds,” *Sci. Robot.*, vol. 8, no. 80, p. eadf0970, 2023.
- [51] W. Xu, Y. Cai, D. He, J. Lin, and F. Zhang, “Fast-lio2: Fast direct lidar-inertial odometry,” *IEEE Trans. Robot.*, vol. 38, no. 4, pp. 2053–2073, 2022.
- [52] A. Hornung, K. M. Wurm, M. Bennewitz, C. Stachniss, and W. Burgard, “OctoMap: An efficient probabilistic 3D mapping framework based on octrees,” *Auton. Robots.*, vol. 34, no. 3, pp. 189–206, 2013.
- [53] K. Koide, J. Miura, and E. Menegatti, “A portable three-dimensional LIDAR-based system for long-term and wide-area people behavior measurement,” *Int. J. Adv. Robot. Syst.*, vol. 16, no. 2, 2019.

APPENDIX

A. Proof of Lemmas and Theorems

Proof. of Lemma 1. Denote by $t_h^-(n_i)$ and $t_h^+(n_i)$ the time instants immediately before and after the operator h incorporates the received data at the return event c_{h,n_i} . Then, for each $c_{h,n_i} \in \Gamma_h$, it holds that $t_h^j(t_h^+(n_i)) = \max\{t_h^j(t_h^-(n_i)), t^j(n_i)\}$, $\forall j \in \mathcal{N}$, where $t_h^j(t)$ denotes the most recent update time at the operator h for data originating from robot j , and $t^j(n_i)$ is the time-stamp of robot j carried by n_i at the return event. Consequently, $\delta_h(t_h^+(n_i)) = t_h(n_i) - \min_{j \in \mathcal{N}}\{t^j(n_i)\} \leq t_h(n_i) - \chi_{n_i}$, where $\chi_{n_i} \triangleq \min_{j \in \mathcal{N}}\{t^j(n_i)\}$. If conditions (I) and (II) hold, then $\chi_{n_i} > \chi_{n_{i-1}}$ implies $t_h(n_i) - \chi_{n_i} < t_h(n_i) - \chi_{n_{i-1}} \leq T_h$, which yields $\delta_h(t_h^+(n_i)) < T_h$. Moreover, by the monotonicity of $\delta_h(t)$ between consecutive return events, it holds that

$$\begin{aligned} \delta_h(t_h^-(n_i)) &= \delta_h(t_h^+(n_{i-1})) + t_h(n_i) - t_h(n_{i-1}) \\ &\leq t_h(n_i) - \chi_{n_{i-1}} \leq T_h, \end{aligned}$$

which implies $\delta_h(t_h^-(n_i)) \leq T_h$. Therefore, the latency constraint holds at each return event. Furthermore, for any $t \in (t_h(n_{i-1}), t_h(n_i))$, it follows that $\delta_h(t) \leq \delta_h(t_h^-(n_i)) \leq T_h$. This completes the proof. \square

Proof. of Lemma 2. Consider one execution of $\text{PairCoord}(\cdot)$ between robots i and j . The while-loop removes exactly one task f^* from the unsigned set \mathcal{F}^- at each iteration, hence $|\mathcal{F}^-|$ strictly decreases and the loop terminates in at most $|\mathcal{F}^-|$ iterations, proving finite termination. It remains to show that the returned event c_{ij} is feasible, i.e., satisfies (11). After the return-event stage, either condition (10) holds and no return is appended, in which case the current stamp χ^* already provides a valid upper bound for the next pairing; or a return event is appended to one robot $n \in \{i, j\}$, which updates the stamp to χ^* and yields a conservative feasible upper bound of $T_h + \chi^*$ for subsequent coordination. In the task-sequence stage, p_{ij} is recomputed from $\text{TSP-Path}(p_i^{L_i}, \mathcal{F}^-, p_j^{L_j})$ and c_{ij} is

selected on p_{ij} by $\text{SelComm}(\cdot)$. If the loop stops at some iteration, then (11) is satisfied by construction. Otherwise, tasks are removed until $\mathcal{F}^- = \emptyset$, in which case p_{ij} reduces to a direct path connecting $p_i^{L_i}$ and $p_j^{L_j}$, and $\text{SelComm}(\cdot)$ chooses a meeting event c_{ij} on this path that minimizes the resulting coordination time. Since the return-event stage guarantees a feasible schedule under the bound $T_h + \chi^*$ for this worst-case direct coordination, c_{ij} must satisfy (11). Therefore, $\text{PairCoord}(\cdot)$ always returns a feasible plan and a feasible next pairing event. \square

Proof. of Theorem 1. Lemma 2 ensures that each execution of pairwise coordination returns a feasible solution. In other words, every communication event satisfies constraint (11). Therefore, by Lemma 1, the base request $\{\xi_1^k\}$ is fulfilled at all times for each team $\mathcal{T}_k \in \mathcal{T}$. \square

Proof. of Lemma 3. The candidate family $\widehat{\mathcal{G}}_k^\xi$ is finite, and Alg. 2 evaluates one candidate per iteration. The heuristic in (18) determines only the order of evaluation, so all candidates are eventually examined and the request-instantiation procedure terminates in finite time. For each candidate for which (16) returns $(T_{\text{trs}}, \widehat{\pi}_k^\xi)$, the corresponding detach-execute-rejoin transition is executable by construction. Then LBAP in (17) returns the bottleneck-minimizing assignment Π_k^ξ for that detach schedule. Hence, each such candidate admits a well-defined exact value of (14). Since Alg. 2 updates the incumbent using this exact objective value and exhausts the candidate family, the returned solution is executable under the detach mechanism and minimizes (14) over all candidates for which (16) returns a timed detach schedule. \square

Proof. of Theorem 2. Since the arrival sequence of request bundles is finite, only finitely many requests can be introduced during execution. Consider first a request-activation event. Whenever a request becomes admissible under the sequential compatibility logic of MoRoCo , Alg. 3 invokes the request-instantiation procedure $\text{GraphMatch}(\cdot)$ as in (25). By assumption, this returns an executable detach schedule for the corresponding robot set, together with an instantiated request subgraph and an updated remaining wheel backbone. Hence, after instantiation, the embedded graph still admits the decomposition in (23), namely a remaining wheel component plus the collection of active request subgraphs. If a request is not admissible, it is deferred and the embedded graph remains unchanged. Therefore, after each request-activation event, the embedded graph remains feasible for subsequent coordination.

Next consider a request-completion event. By assumption, every instantiated request subgraph completes its assigned request and rejoins the wheel backbone in finite time. Then, according to Alg. 3, the associated subgraph is removed and its robots are merged back into the wheel component. Thus, after each completion event, the embedded graph again satisfies (23). This proves Item I. Since only finitely many requests arrive, and each instantiated request is completed and removed in finite time, every admissible request that is instantiated by Alg. 3 is serviced in finite time, which proves Item II. The special operator-relocation request $\{\xi_3^k\}$ is deferred while the fleet is split, and becomes admissible once

all active request subgraphs have rejoined and the complete wheel backbone is restored; it is then handled by the same argument. Finally, because only finitely many requests can be instantiated and each active request subgraph disappears after finite-time completion, the number of active request subgraphs decreases to zero after finitely many completion events. Consequently, there exists a finite time t_f such that $\mathcal{G}_k(t) = \mathcal{G}_k^w$ for all $t \geq t_f$. This proves Item III. \square